IEEE Access
Multidisciplinary | Rapid Review | Open Access Journal

Received May 21, 2020, accepted June 14, 2020, date of publication June 22, 2020, date of current version July 2, 2020.

Digital Object Identifier 10.1109/ACCESS.2020.3004056

A Review on Recent Progress in Thermal Imaging and Deep Learning Approaches for Breast Cancer Detection

ROSLIDAR ROSLIDAR[1,2], (Member, IEEE), AULIA RAHMAN[2], (Member, IEEE), RUSDHA MUHARAR[2], (Member, IEEE), MUHAMMAD RIZKY SYAHPUTRA[2], (Member, IEEE), FITRI ARNIA[2], (Member, IEEE), MAIMUN SYUKRI[3], BISWAJEET PRADHAN[4,5], (Senior Member, IEEE), AND KHAIRUL MUNADI[2], (Member, IEEE)

[1]Doctoral School of Engineering Science, Universitas Syiah Kuala, Banda Aceh 23111, Indonesia
[2]Department of Electrical and Computer Engineering, Universitas Syiah Kuala, Banda Aceh 23111, Indonesia
[3]Medical Faculty, Universitas Syiah Kuala, Banda Aceh 23111, Indonesia
[4]Centre for Advanced Modelling and Geospatial Information Systems (CAMGIS), Faculty of Engineering and IT, School of Information, Systems and Modelling, University of Technology Sydney, Ultimo, NSW 2007, Australia
[5]Department of Energy and Mineral Resources Engineering, Sejong University, Seoul 05006, South Korea

Corresponding author: Khairul Munadi (khairul.munadi@unsyiah.ac.id)

This work was supported in part by the Ministry of Education and Culture of the Republic of Indonesia under 2020 Doctoral Research Grant (Hibah Penelitian Disertasi Doktor) and by the Ministry of Research, Technology, and Higher Education of the Republic of Indonesia under 2019 World Class Professor (WCP) Programme.

ABSTRACT Developing a breast cancer screening method is very important to facilitate early breast cancer detection and treatment. Building a screening method using medical imaging modality that does not cause body tissue damage (non-invasive) and does not involve physical touch is challenging. Thermography, a non-invasive and non-contact cancer screening method, can detect tumors at an early stage even under precancerous conditions by observing temperature distribution in both breasts. The thermograms obtained on thermography can be interpreted using deep learning models such as convolutional neural networks (CNNs). CNNs can automatically classify breast thermograms into categories such as normal and abnormal. Despite their demostrated utility, CNNs have not been widely used in breast thermogram classification. In this study, we aimed to summarize the current work and progress in breast cancer detection based on thermography and CNNs. We first discuss of breast thermography potential in early breast cancer detection, providing an overview of the availability of breast thermal datasets together with publicly accessible. We also discuss characteristics of breast thermograms and the differences between healthy and cancerous thermographic patterns. Breast thermogram classification using a CNN model is described step by step including a simulation example illustrating feature learning. We cover most research related to the implementation of deep neural networks for breast thermogram classification and propose future research directions for developing representative datasets, feeding the segmented image, assigning a good kernel, and building a lightweight CNN model to improve CNN performance.

INDEX TERMS Breast cancer, convolutional neural network, deep learning, early detection, thermogram.

I. INTRODUCTION

Global cancer data show that breast cancer is the second most lethal form of cancer worldwide after lung cancer [1]. In 2018, 2 billion new cases of breast cancer were reported worldwide, where 627,000 deaths. A study in Australia [2] showed that breast cancer survival is strongly associated with the size of the tumor at the time of detection, with the size less than 10 mm, the probability of patient survival is 98%. A cohort study showed that 70% of breast cancer cases are detected when the tumor size was 30 mm [3]. Breast cancer usually becomes detectable during screening when

The associate editor coordinating the review of this manuscript and approving it for publication was Gustavo Callico.

the tumor is at least 20 mm in size [4]. Therefore, enabling early detection of breast cancer is crucial to facilitate early treatment.

Early treatment may be beneficial following identification through screening examinations such as clinical-breast examination (CBE) and breast self-examination (BSE). CBE is a regular medical examination performed by healthcare professionals to detect breast lesions, whereas BSE is conducted by an individual to observe physical changes and appearance of breasts. The practice of BSE empowers women to take responsibility for their health. Consequently, BSE is recommended by the World Health Organization for raising awareness among women at risk [5].

Screening methods produce medical images of breasts. The interpretation of these images is normally performed by human experts such as radiologists and doctors. Research shows that the low diagnostic accuracy of thermograms is attributed to weak technical ability and expertise in interpreting such images. The emergence of various diseases and limited human labor has motivated researchers and medical personnel to use computer-assisted technology to facilitate breast thermography-based diagnosis and thus minimize errors. Therefore, a computer system that can automatically classify thermograms into normal and abnormal categories is required. Considering this requirement, research toward finding computer-based solutions to classify medical images has been continuously growing.

Many computer-asisted methods of diagnosis have been developed to assist doctors in interpreting the medical images. During the last decade, significant effort has focused on the development of deep learning (DL) models. Because DL models are publicly available, they can be applied easily using pre-trained networks. In breast cancer detection, many studies are based on DL using mammograms [6]–[17], histology images [18]–[21], tomosyntheses [22]–[25], and ultrasound images [26] have shown satisfactory accuracies.

In contrast, relatively few studies have contributed to non-invasive thermal of breasts using the deep neural network (DNN) technique. Considering current limited resources, the work on this problem is still at its early stages. Hence significant effort is required to develop reliable non-invasive computer-assisted technology to enable the early detection of breast cancer. This necessitates a study of relevant previous, current, and necessary future research on thermal imaging and DL for breast cancer detection should be considered of paramount importance. Potential research could be directed and focused on the substantial outstanding issues identified in this study.

In this study, we review current progress in breast cancer detection using DL and thermography as a non-invasive approach. We also highlight necessary future research directions to improve the accuracy of breast cancer detection using thermal imaging and DL. The state-of-the-art and contributions of this paper can be summarized as follows:

- An overview of breast thermography potential for cancer detection including the availability of the breast thermogram dataset.
- Step-by-step explanation of the CNN concept.
- Simple visualization in feature learning for breast cancer thermograms.
- A review of the latest progress in thermal imaging and DL approaches for the early detection of breast cancer.
- To propose the potential research challenges in developing a fast and an accurate CNN-thermal imaging system for breast cancer detection.

This study is organized as follows. Section II presents a review of the available breast cancer screening methods. Section III explains the concepts involved in breast thermal imaging and its potential for breast cancer detection. The availability of breast thermogram datasets is explained. We also outline the characteristics of healthy and cancerous breast thermograms. Section IV describes the state-of-the-art of CNN as the well-known image classifier in the DNN model for thermal breast cancer detection. In Section V, we discuss previous research on breast thermogram classification using artificial neural network algorithms and CNN models. Finally, the manifold challenges in future research, particularly to improve the accuracy and training speed of CNN models are highlighted in Section VI.

II. STANDARD SCREENING METHODS

Breast cancer risk assessment is critical for identifying women who may benefit from more intensive breast cancer surveillance [27]. Prior to surveillance, one must undergo a screening test. Currently, the gold standard screening method for early breast cancer detection is mammography [28], an X-ray examination, where the breast is placed on a stand and pressed by a disc to spread the breast tissue evenly and capture characteristics of microcalcification [29]. Similar to all X-ray imaging, mammography involves the use of doses of ionizing radiation to create images. Repeated mammography screening may increase breast cancer risk due to exposure to ionizing radiation [30]. A previous study indicated that each exposure to X-rays increases breast cancer risk by 2% [31].

Another screening technique that uses a small amount of radioactivity is positron emission tomography (PET). Radioactive materials termed radiotracers or radiopharmaceuticals are injected into the body, such that a part of the body with greater absorption of radioactive tracers may indicate disease. PET combined with computer tomography (CT) allows the retrieval of information about the size, shape, and location of a tumor. Although examination using PET/CT is non-invasive but the injection procedure is invasive and the use of radioactive material can be harmful to the patients.

A non-invasive ultrasound breast screening method uses high-frequency sound waves that bounce off the breast tissue and are collected as an echo to produce an image. This technique has limitations in identifying calcifications in women age above 40 years. When performing ultrasound, specific

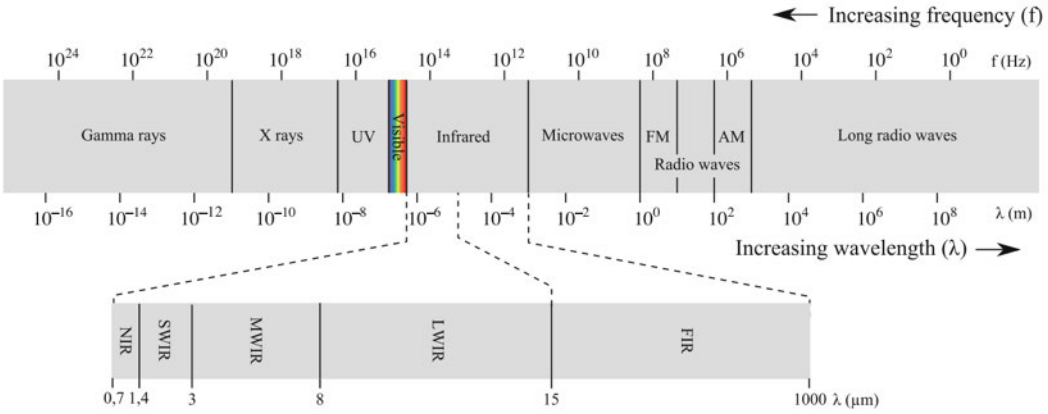

FIGURE 1. Electromagnetic wave spectrum [39].

and improved anatomical knowledge is required as a formal educational program.

Early detection of breast cancer can also be achieved using magnetic resonance imaging (MRI) [32], PET/CT [33], and ultrasound [34]. Using radio waves and magnetic fields, breast images are obtained when diagnostic mammography cannot identify a tumor or other possible growth of a lump in mammograms. MRI scanning is well-adapted to studying soft tissues. However, in some patients, the procedure can cause claustrophobia and the procedure involves high expenses.

Recently, a screening method called thermography was promoted as a risk-free, low-cost, non-contact imaging technique. Thermography is a non-invasive breast cancer screening approach that uses a thermal camera to capture breast images [35]. It allows early detection using thermal anomaly information of breast asymmetry. Breast cancer can produce variations in the mammary thermal pattern prior to clinical and mammographic changes (visible breast tissue on a mammogram) [36]. As also reported previously [37], thermography can detect breast cancer up to 10-years earlier than mammography; however, thermography has a high false positive rate depending on the classification technique used for interpretation [38]. Consequently, a reliable classification method for breast thermograms is necessary.

III. BREAST THERMAL IMAGING MODALITY

Infrared waves are within the wavelength range of light and microwaves. All objects can emit infrared radiation as a function of the temperature of that object. Heating an object increases the amount of infrared radiation released and causes it to propagate in shorter waves [40].

Figure 1 shows the electromagnetic spectrum. Infared wavelength, which are not visible to the human eye, can be captured using infrared detectors and cameras. Infrared radiation generally covers wavelengths from 0.75 to 1000 μm, whereas the wavelengths emitted by the human body during diagnostic measurements are at narrow-band wavelengths, 8 to 12 μm, which are termed the long-wave infrared (LWIR). In medical infrared imaging, this range is known as thermal infrared (TIR). Within this range, infrared emission usually occurs as heat or thermal radiation, the measurement of which is termed thermography. The image produced by TIR imaging is called a thermogram [39]. This infrared wave cannot be visually observed because it lies outside the wavelength of visible light, but it can be captured using a thermal camera.

A. POTENTIAL OF BREAST THERMOGRAM MODALITY

In general, thermography has two advantages. First, its thermographic nature, which is non-invasive and enables visualization and quantification, facilitates risk-free detection of breast cancer. Second, thermography facilitates real-time imaging, allowing data storage on a computer, which can later be used for data processing [41]. Despite these advantages, thermography is not considered as a replacement for mammography. As discussed previously [42], mammography remains the gold standard screening technique and offers an effective means for early breast cancer detection. However, certain factors can affect the diagnostic accuracy of mammography [43]. First, mammography primarily depends on structural distinction and anatomical variation of the tumor from the surrounding breast tissue. Second, mammography sensitivity is higher for older women (60–69-years) than for younger ones (less than 50-years).

Comprehensive research concerning the medical imaging modalities for diagnosing breast cancer [46] suggests that thermography is a superior imaging modality for dense breast tissues and their early detection. This finding is supported by previous research [47] which indicated that thermography could be correct from 8–10 years before mammography can detect a mass. Furthermore, mammography has difficulties in reading a large, dense, and fibrocystic breasts. As discussed in a previous study [48], to reliably detect tumors using X-rays, the density of the lump should be more than that of the surrounding tissue. Consequently, mammography is mainly applicable to a woman aged above 45-years. As reported previously [49], the average size of tumors undetected by

thermal imaging and mammography is 1.28 and 1.66 cm respectively indicating that thermography can facilitate earlier tumor detection.

Nevertheless, a further study [50] did not recommend the use of digital infrared thermal imaging (DITI) for women with a history of a surgery or core biopsy, despite the fact that it is non-invasive and painless. This is due to the low sensitivity of DITI hindering its recommendation as a primary evaluation or routine basic screening for breast cancer.

A study [51] compared the accuracy of thermography and mammography in detecting breast cancer verifying that the accuracy of mammography is higher than that of thermography (76.9% versus 67.7%). In conclusion, at that time thermography could not replace mammography as an early breast cancer detection method. However, the use of thermography as a companion to mammography is highly recommended to obtain maximum test results.

B. BREAST THERMOGRAPHY

As discussed in [52], changes in temperature distribution are a symptom of abnormality in body tissues. A study also confirm that the thermal distribution of cancerous breast and tumor volume fraction in the heterogeneous zone influences the breast surface temperature [53]. However, given the limitations of the human visual system such temperature differences are difficult to detect. Therefore, a system that can detect changes in temperature distribution is required.

In 1957, a study [54] reported thermography as a new tool for investigating breast lesions. Infrared photons represent only a narrow-band of the electromagnetic spectrum, but the information contain within these images is fundamentally associated with the functional status and movement in the body [55]. Following several decades after the development, a new system for acquiring surface thermal patterns of the breast and image interpretation was developed [56] and termed thermal texture mapping. Thermal texture maps were introduced in 2004 to solve the inverse problem of the heat transfer equation by locating inner abnormal heat sources and their metabolic status [57].

In 2017, a complementary non-invasive tool for thermogram acquisition was introduced [44]. Its proposed protocol is shown in Figure 2. In this method, the IR thermographic device is placed 1.2 m away from the relaxed seated patient.

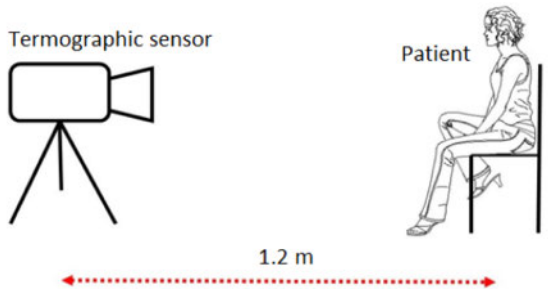

FIGURE 2. Thermogram acquisition setting [44].

At this distance, the minimum measurable spot size is 0.5 cm, which allows the measurement of cancer tumors sized larger than 0.5 cm. Two types of protocol may be employed in capturing the image: static and dynamic protocols. The static protocol involves a single image captured after 10–15 minutes of thermal stabilization during rest, whereas the dynamic protocol involves a series of thermograms captured every 15 seconds during five minutes.

In the same year, Bhowmik *et al.* [58] also proposed a standard breast thermogram acquisition protocol. Factors influencing thermography such as patient's personal and medical information as well as room condition were adjusted before the examination. The acquisition of breast thermograms was conducted in a black cubicle to acquire a homogeneous background. A bed-cum-table was designed to assure acclimation among patients, who were asked to lie down for 15 minutes. Patients were positioned 1 meter away from the thermal camera except those with a larger-than-average body anatomy and the best-fitting distance was determined. Images were captured in the supine, frontal, left lateral, right lateral, left oblique, and right oblique views.

Figure 3 shows the thermograms of normal and abnormal breasts, with the latter indicating a disease state, downloaded from the DMR database [45]. These images show three patients with different medical histories. Figure 3(a) shows an image of a healthy patient having undergone no previous screening test. Figure 3(b) shows an image of a healthy patient with a history of no complaints and symptoms, but with warts on the left breast; this patient had undergone mammography. Figure 3(c) shows an image of a patient with cancer who had undergone biopsy of the left breast. The varying temperature distributions among these different case images are clearly noticeable. These variations are an important signature of breast thermogram for breast cancer detection.

It is important to note that the menstruation cycle must be considered when conducting thermography. A study [38] found that a patient on the 20th day of the menstruation cycle has an unstable body temperature resulting in false-positive interpretation of her breast thermogram. Hence, thermography is recommended to be performed within the 5th and 12th or on the 21st day of menstruation to avoid false interpretation.

C. BREAST THERMAL DATASET

Several studies on breast thermogram acquisition have been conducted during the last decade. As shown in Table 1, the first dataset [59] was selected from images taken in 1984 by Dr. Monique Frize and her team, using the first generation thermographic camera Thermovision 680 Medical (Agatronics) connected to an OSCAR 780 (Agatronics).

Unlike the large number of mammograms that are stored in public digital databases, breast thermograms are stored mainly in private databases. Currently, relatively few public breast thermogram databases are available, e.g. PROENG [65] and Silva *et al.* [45]. Other online datasets

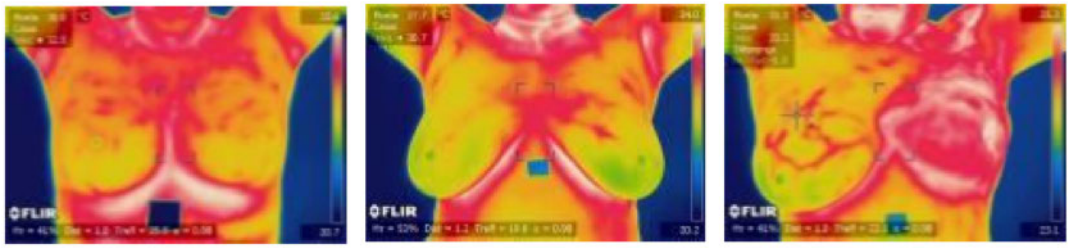

FIGURE 3. Breast thermograms downloaded from Database for Mastology Research (DMR) [45].

TABLE 1. Breast thermogram dataset.

Study	Number of Patients	Classes	Tools
Koay [59]	19 patients (selected from 86 images)	14 without pathology 5 with pathology	Thermovision 680 Medical
Ng and Kee [60]	90 patients	30 asymptomatic 48 benign 4 cancer	Camera Avio TVS-2000 MkII ST
Arora et al. [61]	94 biopsy patients	60 malignant 34 benign	Sentinel BreastScan™
Tang et al. [62]	117 patients	47 malignant 70 benign	TSI-21 Thermographic System
Wishart et al. [63]	106 biopsy patients	65 malignant 41 benign	Sentinel BreastScan™
Nurhayati et al. [64]	150 women	50 healthy 50 chemotherapy 50 advanced	Digital thermal camera Fluke
PROENG [65]	220 patients		FLIR Therma-CAM S45
Silva et al. [45]	285 ID patients	186 healthy 44 sick 55 unknown	FLIR Thermal Camera SC620
Bhowmik et al. [58]	100 subjects	45 healthy 36 benign 13 malignant 6 unknown	FLIR T650sc

include those used previously [66] from Ann Arbor Thermography [67], the Thermal imaging lab in the San Francisco Bay Area [68], the American College of Clinical Thermology [69], Thermography of Iowa [70], and Sunstate Thermal Imaging Center in Australia [71].

We suggest that more studies of breast thermogram acquisition with universal standards should be undertaken in the future to support specialists and researchers in their educational and research activities. Moreover, datasets are the primary concern in the training processes of DNNs.

D. BREAST THERMAL FEATURE

A feature is any distinctive aspect or characteristic that is used to solve a computational task related to a certain application. Each breast has particular thermographic characteristics or patterns that do not change over time [38]. Slight temperature variation in breasts indicates new developments in the breasts and warrant further examination. This is based on the assumption that breast temperature should be symmetrical. Thus, if one breast has cancerous cells, then the two breast thermograms would deviate from each other. In general, the highest average mean temperature deviation of the patient with breast cancer and the benign is 0.51°C, and with the healthy one is 0.85°C [35].

The symmetry of breast thermograms is described by the image features which can be used as parameters to classify the thermograms of patients with and without cancer. Regarding DL, such features will be used as inputs for the classification algorithm. Thus, it is important to identify image features that uniquely describe the symmetry pattern of breast thermal distribution.

A study [72] proposed a statistical method to identify parameters that best distinguish healthy, benign, and malignant groups of patients. First, the correlation coefficient of the variable mean, standard deviation, median, and mode of the temperature was calculated and tested for significance. The results showed that the mean, median, and mode have a low correlation coefficient among the healthy, benign, and carcinoma cases but a high correlation between breasts in individual groups. However, the standard deviation shows a low correlation between the breasts of each case. Second, using descriptive statistics, the histograms of each breast were obtained. The histograms of the carcinoma case showed a significantly different skewness and mean temperature compared with those of normal and abnormal breasts. Figure 4 compares the histograms of healthy and cancerous thermograms to illustrate their differing temperature distributions. Figure 4(a) shows an image of a healthy patient indicating no significant differences in the histograms of both breasts. However, Figure 4(b) shows an image of the patient with cancer on the left side of the breast. The temperature distribution is asymmetrical and has a different mean temperature compared with those of normal side.

An investigation to determine the breast thermogram signatures was further conducted [73] and first- and second-order of the statistical parameters were analyzed. The investigation confirmed that among the analyzed first-order parameters, only mean and skewness were promising for

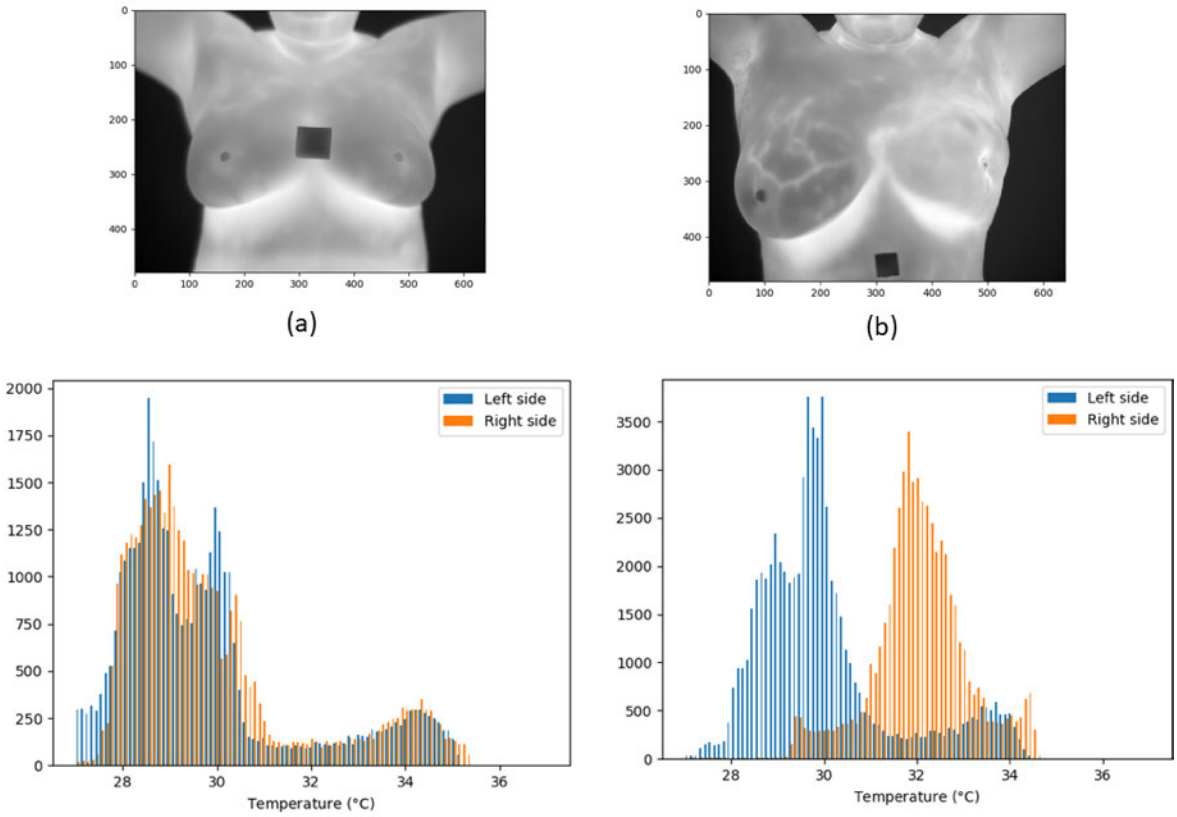

FIGURE 4. The histogram of a) healthy and b) cancer thermograms.

successful classification of breast thermograms, but they were not effective for separating breast thermograms with and without tumors when used as inputs for NNs. On the other hand, the second-order approach (co-occurrence matrix) provided better results because its difference variance and variance allow the separation of almost all healthy and malignant tumor cases.

In Table 2, we present first-order histogram based features and co-occurrence matrix based features. An image is assumed as the function $f(x, y)$ of two space variables x and y. The value of the function is any discrete value of i within the range $i \in [0, L-1]$. For the first order histogram based features, the intensity-level histogram is [74],

$$h(i) = \sum_{x=0}^{N-1} \sum_{y=0}^{M-1} \delta(f(x, y), i) \tag{1}$$

where δ is the Kronecker delta function,

$$\delta(j, i) = \begin{cases} 1, & j = i \\ 0, & j \neq i \end{cases} \tag{2}$$

and $p(i)$ is the probability value of image intensity,

$$p(i) = \frac{h(i)}{NM}. \tag{3}$$

The co-occurrence matrix, $h_{d\theta}(i, j)$, is calculated as described previously [75]. Co-occuring values of i and j are counted when two pixels with distance d and direction θ exist. This could result from a symmetric pairs separated by d and $-d$ or not symmetric pairs separated by d distance. When the co-occurence matrix $h_{d\theta}(i, j)$ is divided by the number of neighbouring pixels $R(d, \theta)$ in the image, the matrix becomes an estimate of joint probability, $p_{d\theta}(i, j)$. For image $f(x, y)$ with a set of L discrete intensity levels, the matrix $h_{d\theta}(i, j)$ is defined such that its (i, j)th entry is equal to the number of times that $f(x_1, y_1) = i$ and $f(x_2, y_2) = j$, where

$$(x_2, y_2) = (x_1, y_1) + (d \cos\theta, d \sin\theta). \tag{4}$$

A study applied both histogram statistical and gray-level co-occurrence matrix (GLCM) for the identification of textural features of breast thermograms [76]. Features of segmented breast thermograms were extracted using the first-order statistics of entropy, kurtosis, mean, skewness, standard deviation, and variance. On the other hand, in GLCM, entities of contrast, correlation, energy, and homogeneity were used to describe the texture feature. The mean value was the most significant value of the first-order statistics to separate cancerous and healthy thermograms. In texture-related GLCM, contrast, homogeneity, and energy were justified as the most distinctive values distinguishing healthy and cancerous thermograms.

TABLE 2. First-order histogram and co-occurrence matrix based features [74].

First-order histogram based features	Co-occurrence matrix based features
Mean, $\mu = \sum_{i-0}^{L-1} ip(i)$,	Energy, $E = \sum_{i=0}^{L-1}\sum_{j=0}^{L-1} p^2(i,j)$,
Variance, $\sigma^2 = \sum_{i=0}^{L-1} (i-\mu)^2 p(i)$	Inertia = $\sum_{i=0}^{L-1}\sum_{j=0}^{L-1} (i-j)^2 p(i,j)$
Skewness, $\mu_3 = \sigma^{-3}\sum_{i=0}^{L-1} (i-\mu)^3 p(i)$	Difference variance = $Var(p_{x-y})$,
Kurtosis, $\mu_4 = \sigma^{-4}\sum_{i=0}^{L-1} (i-\mu)^4 p(i) - 3$	Correlation = $\frac{\sum_{i=0}^{L-1}\sum_{j=0}^{L-1}(i,j)p(i,j)-\mu_x\mu_y}{\sigma_x\sigma_y}$
Energy, $E = \sum_{i=0}^{L-1} p^2(i)$	Inverse Difference = $\sum_{i=0}^{L-1}\sum_{j=0}^{L-1} \frac{p(i,j)}{1+(i-j)^2}$
Entropy, $H = -\sum_{i=0}^{L-1} p(i)\log_2(p(i))$	Entropy, $H = -\sum_{i=0}^{L-1}\sum_{j=0}^{L-1} p(i,j)\log_2[p(i,j)]$

IV. DEEP LEARNING FOR BREAST THERMOGRAM CLASSIFICATION

The neural network is inspired by how neurons in the human brain work. Each neuron in the human brain is interconnected and information flows across each of these neurons. In NNs, each neuron receives input and performs a dot operation with weights and biases. Weight specifies the strength of the connection between two nodes. Biases are external values that increase or decrease the net input of the activation function [77]. Nodes are the individual processing units in each layer. Figure 5 illustrates the mathematical model of a neuron.

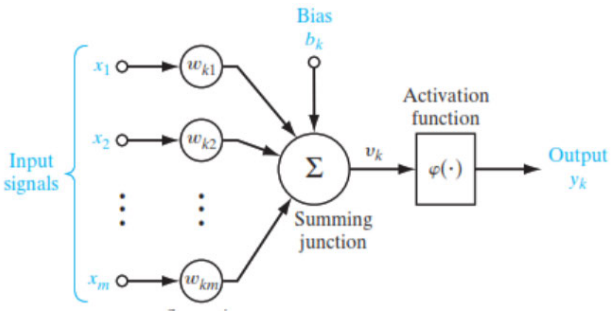

FIGURE 5. Neural Network resembles human nerves system [78].

A neural network comprises neurons or units with activation function $\varphi(.)$ and parameter $\theta = \{\mathbf{W}, \mathbf{B}\}$, where $\mathbf{W}$ is the vector of weights (kernel) and $\mathbf{B}$ is the vector of biases. Equation (5) represents the convolution operation [77]:

$$y = \sum_i w_i x_i + b = \varphi(\mathbf{W}^T\mathbf{x} + \mathbf{B}). \tag{5}$$

The activation function expresses a linear combination of input $\mathbf{x}$ with respect to neurons and parameters, followed by an element-wise nonlinearity. The transfer or activation function determines whether or not the neuron "active" based on the weighted sum of the input.

Learning from data has two main goals: to understand the data generation process and data interpretation; and to predict future observations. Predicting future projects does not require a probabilistic accuracy rate. However, accuracy is a focus of medical data interpretation. As applied in detecting breast cancer, 100% accuracy is required to ensure that the diagnosis follows the ground truth.

Neural network is a massive parallel distributed processor made up of simple processing units, which has a natural propensity for strong experiential knowledge, making it available for use. The NN algorithm allows the learning of the qualitative value of an image. Thus, it is appropriate for application in breast thermogram classification.

A convolutional neural network (CNN) is a deep neural network algorithm that processes input images by assigning certain learnable weights and biases to map important features that differentiate one image from others. In this way, the classification result can be observed as the output. Figure 6 shows the general architecture of CNNs for classifying the breast thermograms into two classes, healthy and cancer. Three major considerations must be made: dataset preparation in image pre-processing, feature learning, and classification. The classification can be binary (healthy and cancer), or more classes such as healthy, benign, and malignant. In the following sections, we review the concepts and related efforts in CNN implementation for breast thermogram classification.

A. IMAGE PRE-PROCESSING

Image pre-processing aims to improve image data/features by suppressing unwanted data and enhancing important image features to increase the performance of the NN model. Image pre-processing is crucial for NNs given that the success of the learning process depends on feature learning from input images. Generally, image pre-processing includes mean

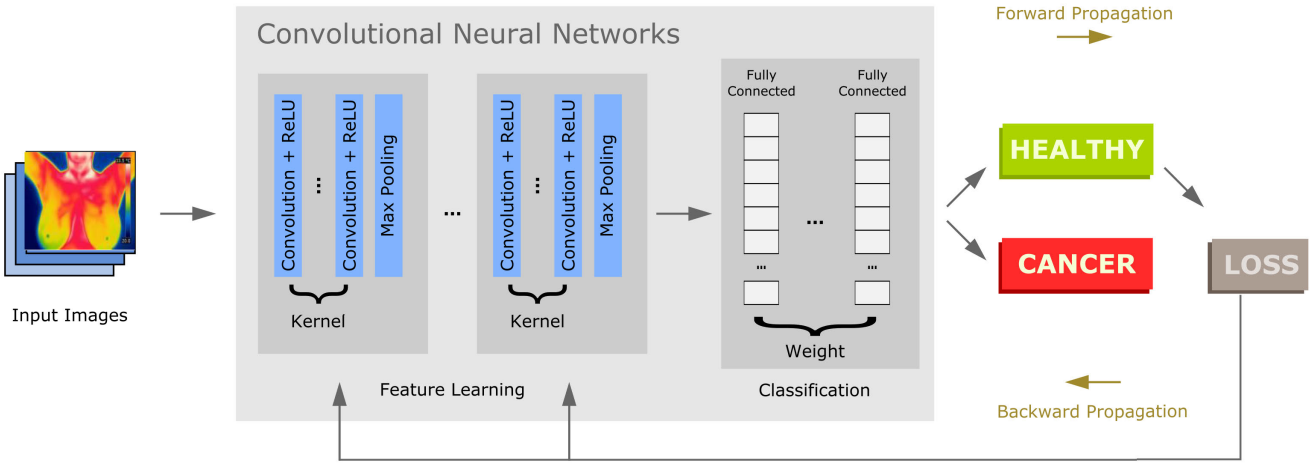

FIGURE 6. Convolutional Neural Networks for BC early detection using breast thermograms.

subtraction, normalization, PCA whitening, and local contrast normalization [79].

The normalization of the breast thermogram temperature matrix was undertaken previously [80]. The study compared the classification accuracy of normalized datasets with the non-normalized breast thermogram temperature matrix. The result showed that the normalized input has a 16% better accuracy rate than the non-normalized input.

In addition, common techniques used for breast thermogram pre-processing include resizing, segmentation of the region of interest (ROI), and augmentation. Image resizing aims to provide the base size for all input images. The size of the image comprises its weight; height; and the number of red, green, and blue (RGB) channels. For example, given that the breast thermogram has three RGB channels, its size is $224 \times 224 \times 3$ with a square size weight and height of 224.

Image segmentation considers only ROI and eliminates the rest of the image. The ROI of the breast thermogram should include half of the armpit such that all breast tissue and nearby ganglion groups are analyzed [35]. A review of ROI extraction in thermography images for the medical purposes can be found in previous study [81]. Automatic segmentation approaches lead to fast and highly reproducible analysis; thus, it is essential to standardize the anatomical landmarks of ROI to the edges of the image during acquisition. The characteristic points chosen prior to developing automatic segmentation are as follows [81]:

- thermal features or local thermal patterns because the temperature distribution pattern is different and invariant in contrast to those of the adjacent regions.
- topographic anatomy, geometric shape, and arrangement of well-defined anatomical landmarks.
- anthropometric ratios, such that different body proportions show a mutual agreement.

The segmented ROI of a breast thermogram shows a significant increase in temperature compared with that in the neighboring area. As noted in Table 3, various segmentation techniques were applied to determine the best method to produce ROI to allow optimum feature extraction. The asymmetry of breasts with cancer drives breast thermogram segmentation to detect the bifurcation line of the right and left breasts.

The most challenging part of breast segmentation is identifying the lower breast boundaries and inframammary folds due to limitations of low contrast. Suganthi and Ramakrishnan [88] proposed anisotropic diffusion filter integration with the level set framework to avoid smoothing across the boundary and preserve sharp boundaries. The similarity of segmented ROIs and the ground truth images achieves average accuracy of 98%. The level set method was improved by Golestani [66], for high accuracy with minimum computation time.

Sathish *et al.* [89] showed tracing shape edges by applying a polynomial curve fitting. This method was able to detect slight concavities in the upper border and convexities in the lower part. The algorithm was claimed to work more rapidly than the Hough transformation that is commonly used for curve extraction.

Pramanik *et al.* [91] proposed a new multiscale local intensity measurement function (multisclae spatially weighted pixel-contribution and shape-feature-embedded force, MSPSF) to manage complexity arising from intensity non-uniformity and noise. Segmentation was undertaken in two steps: MSPSF energy functional and MSPSF-based level set methods. The MSPF energy functional-based level set method was used to compute the intensity distribution of the region and produce sharp discontinuities. The level set method worked in two stages, to automatically initialize the complex intensity distribution of breast thermograms and minimize energy. The proposed segmentation method was found to reduce computation time. In another proposed segmentation method, Pramanik *et al.* [92] used arc-approximation to identify the upper boundary of the breast alongside triangular-space search (BATS) to trace

TABLE 3. Segmentation of breast thermogram.

Study	Techniques	Segmented area
Lipari and Head [82]	Semi-automatic segmentation	Each breast is divided into four quadrants by drawing a polygon around each breast region
Scale et al. [83] Schaefer	1) Manual segmentation 2) Canny edge 3) Hough transform 4) Interpolation empirical rules	1) Remove body borders (shoulders and waist) 2) Bottom breast boundary 3) Identify curve edge 4) Detect border by curves 5) Breast upper limit
Qi et al. [84]	Edge-based segmentation: Hough transform	Body borders were segmented in two areas based on three key points: • horizontal line from the left to right of the two armpits, • parabolic lines from the left to right boundary with an intersection point. • vertical line passing through the intersection point
EtehadTavakol et al. [85]	Fuzzy C-means	Color segmentation
Jin-Yu et al. [86]	Genetic algorithm with the Otsu Method	Separatation of the region with a higher temperature
Kapoor and Prasad [87]	Automatic segmentation using Canny edge detector and Hough transform	Edge detection to extract breasts boundaries, and Hough transform to extract the lower breast boundaries
Suganthi et al. [88]	Level set method with an anisotropic diffusion filter	The anisotropic diffusion filter handles low contrast of breast thermogram by sharpening edges.
Golestani et al. [66]	Level set method	Extract hot regions by moving the curve within an image at a certain speed toward features of interest such as lines and edges. Finding the optimal segmentation of an image by minimizing functional energy.
Sathish et al. [89]	Applying Canny and Horizontal Projection Profile (HPP)	Canny extracts inframammary curves, and HPP detects inframammary folds
Devi and Anandhamala [90]	Bifurcation point fitting	Identifying curve that passes through the inframammary fold.
Pramanik et al. [91]	Applying three models: 1) Breast blood perfusion (BBP) 2) Adaptive triangular histogram-based thresholding (ATHT) 3) Multiscale spatially-weighted pixel contribution and shape-feature-embedded force (MSPSF)	1) BPP model is used to improve the contrast between the region of abnormality and normal tissue 2) ATHT segments the hottest region 3) MSPSF manages the adverse effect of intensity non-uniformity and noise
Pramanik et al. [92]	Applying novel methods: 1) Arc-approximation 2) Triangular-space search (BATS)	1) Arc-approximation algorithms identify the upper boundary of the breast 2) Iterative adaptive thresholding detects the lower boundary curve (LBC) of the breast region for identifying the inframammary fold region 3) Triangular-space search handles the tracing and extrapolating of the actual LBCs
Koshki et al. [93]	Applying two models for one segmentation process: 1) Extending Contour Level (ECLS) 2) Controlled Chan-Vese	1) ECLS can extract hot regions with different levels of complicated intensity 2) Improving the ECLS output by controlling the evolution of the contour using statistical information from the image.

lower boundary curve of the breast region. However, in some cases, this method failed to segment the breast region accurately.

Instead of the level set method in which an evolving contour moves toward the target boundary, a recent segmentation method proposed by Koshki *et al.* [93] located the initial contour within the desired object and converged to the outside contour pixels with similar intensity to average intensity. This extending contour level set model can extract objects in multi-region images such as breast thermograms.

Another process in preparing the dataset before feeding it to the NN is augmentation. This process aims to deal with

limited datasets. The works in [94] convey four types of data augmentation; horizontal and vertical flip, rotation between 0–45 degrees, 20% zoom, and normalized noise.

The quality of the dataset fed into the NNs also affects the accuracy of image classification. Another study [95] evaluated the visual quality of color image datasets in four DNN models: Caffe Reference [96], VGG-CNN-S [97], VGG-16 [98], and GoogLeNet [99]. The images downloaded from the dataset in a study [100] were conditioned with five types of distortion: JPEG compression, JPEG2000 compression, noise, blur, and contrast. Their subsequent classification confirmed that the accuracy of networks decreases as image quality degrades. The worst falloff occurred in the Caffe and VGG-CNN-S networks. In the deeper networks, i.e. VGG-16 and GoogLeNet, the performance decreased more slowly because the depth structure has more capability in learning image features. This result also demonstrated that noise, contrast, and JPEG distortions significantly degrade classification accuracy.

B. CONVOLUTIONAL NEURAL NETWORKS

NNs are commonly used for recognizing and detecting objects in image input data. In general, CNN is similar to other NNs, having weight, bias, and the activation function when processing inputs. However, CNNs enable feature extraction to learn patterns from high-dimensional inputs. This process is termed convolution and is executed in a convolutional layer (feature extraction layer). As shown in Figure 6, CNN has two major layers: feature extraction and fully connected.

1) FEATURE EXTRACTION LAYER

The feature extraction layer performs encoding to generate image features. Here, one input image is encoded to be a feature map containing numbers that represent image characters. This layer comprises two execution parts: convolution and pooling. The convolution part is structured such that a filter (kernel) with a certain size is formed. Given that the breast thermogram comprises three color channels (RGB), there are three kernels in accordance with the channels.

In simple words, a filter (kernel) slides along the width and height of the input feature map, with each slide denoting the dot product operation of each part of the input feature map with the appropriate kernel value. This operation is called convolution. For example, a 2D input feature map has a size of 4×4 and a convolution filter sized 2×2. The convolution layer multiplies the filter with the same size as the input region by 2×2. This procedure is repeated until the whole input area is multiplied by the filter. The resulting values are summed to generate one output, which is called the feature or activation map. The number of feature maps depends on the size of the kernel.

When creating the convolution operation, we have to consider the size of the stride and padding. Stride is the parameter that determining the steps along the horizontal followed by vertical positions. For example, if the stride is 2, the kernel steps 2 pixels horizontally and 2 pixels vertically [79]. A smaller stride results in more detailed information retrieval; however, not all small sized strides will introduce good performance.

Theoretically, the output dimension will always be smaller than the input dimension, except a kernel sized 1×1 with stride of 1. Given that the output will be used as the input for the next convolutional layer, more information will be rendered unnecessary. To overcome this problem, one can apply padding into the input. Padding is the parameter determining the number of pixels (with zeros) to be added at each side of the input to manipulate the output dimension of the convolutional layer (feature map). By applying padding at all input sides, the output dimension can be set to be equal or to not decreases, allowing the deeper convolutional layer to be applied; this enable more features to be extracted. Padding also improves DNN performance by allowing the convolution filter identify true information among zeros.

The output of the feature layer is a feature map, which is then fed into the pooling layer. The pooling layer comprises one filter with a certain size of stride. In the convolutional layer, feature maps are up-sampled, whereas in the pooling layer, feature maps are down-sampled. In other words, the dimensions of the feature map in the pooling layer are reduced to avoid overfitting. There are two commonly used types of pooling activation functions that are usually being used: max pooling and average pooling. The maximum value of the feature maps is selected in max pooling, whereas the average value of all feature maps is selected in average pooling.

CNN layers are often followed by a non-linear activation function. To overcome this condition, the activation function takes a real-valued input and compresses it within a small range such as [0, 1] and [-1, 1]. The non-linear function allows NNs to learn non-linear mapping. It works as a switch that decides whether or not a neuron activates if provided with certain inputs. Common activation functions used in DNN are the sigmoid, tanh, and ReLu functions [79].

In the learning features, CNNs iterate convolution and max pooling processes many times to recognize the characteristics (features) of the input. Figure 7 illustrates the convolution process in CNN using breast thermograms as the input images. Given that the input has three channels (RGB), the kernel volume also comprises three individual 2D kernels. Each channel convolves with one kernel. The size of the kernel is determined according to the number of feature maps.

Figure 8 shows the visual results of the convolutional stage of NN in learning the features of a cancerous breast thermogram. In total, 32 feature maps were generated by a pre-trained CNN of MobileNetV2 [102] using one breast thermogram. The feature maps are stored in the pooling and the position of a pixel in the activation function of a channel corresponds to the same position in the original image. Each tile in the grid of the feature map represents the convolution

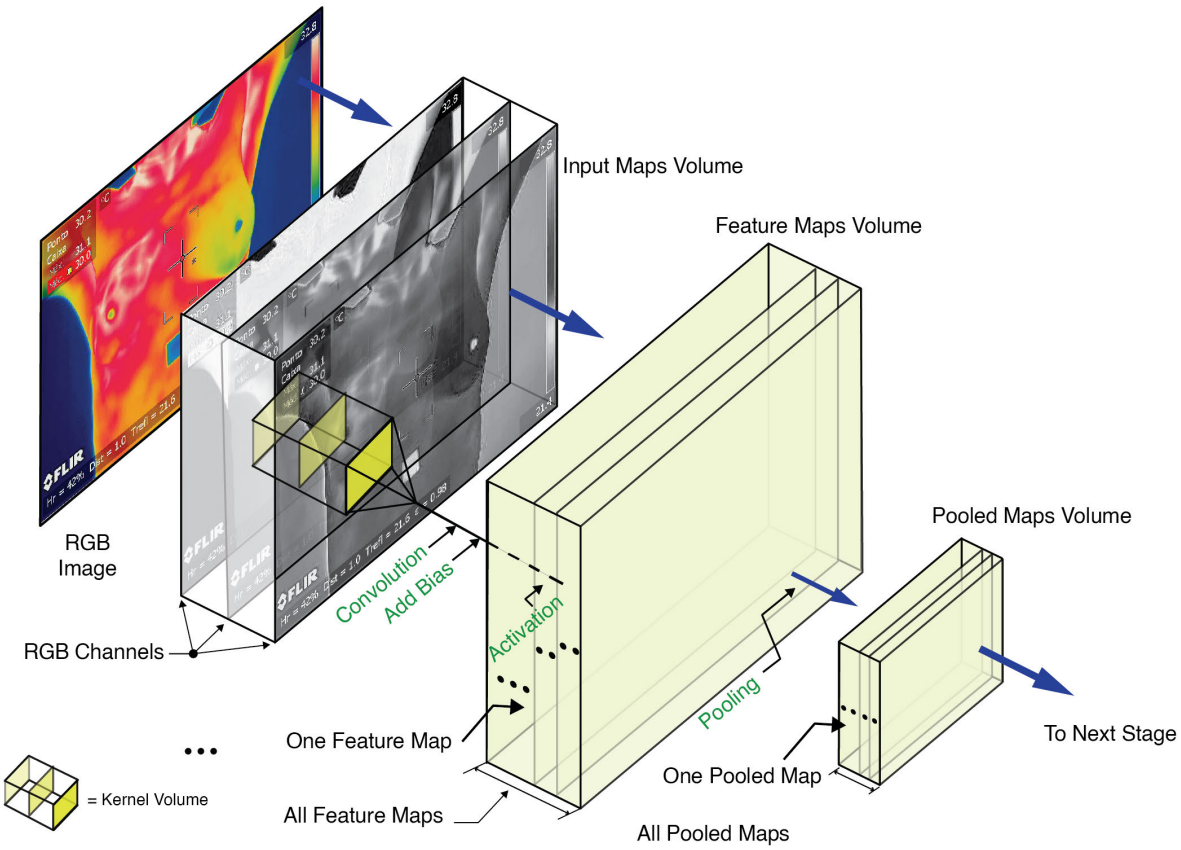

FIGURE 7. Visualization of convolutional process of a cancerous breast thermogram; modified from a previous study [101].

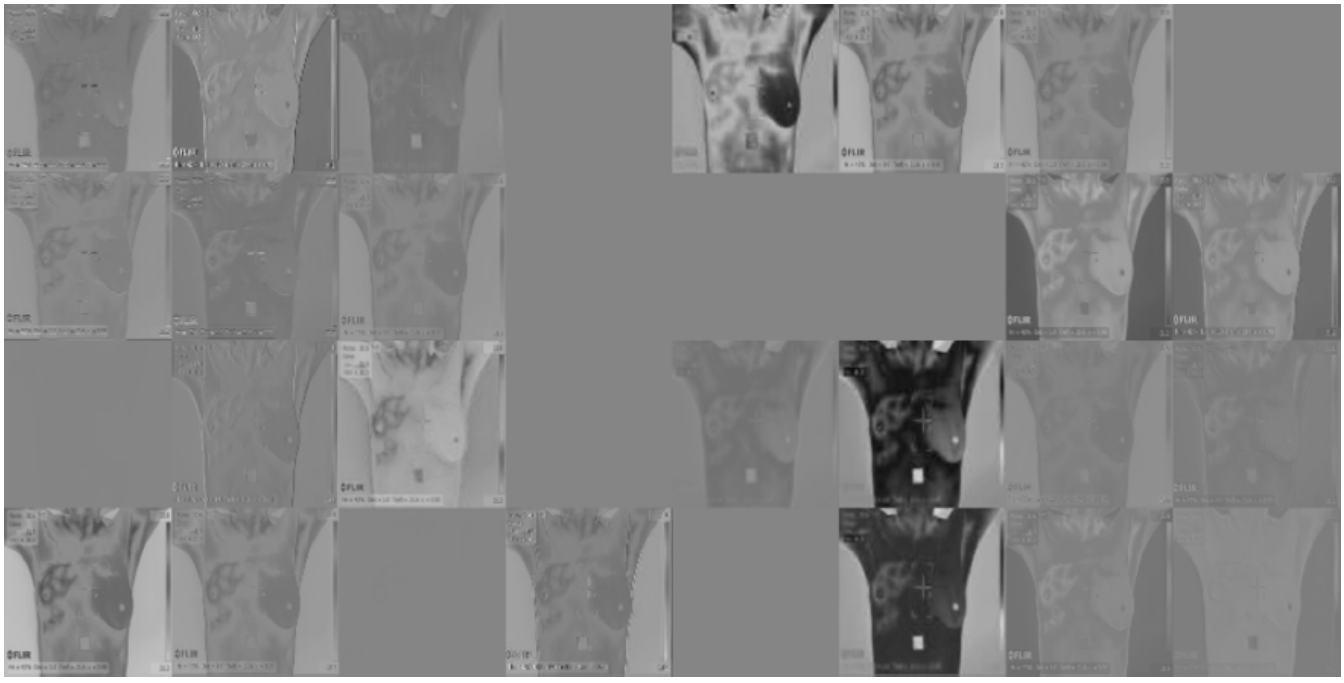

FIGURE 8. Feature mapping of a cancerous breast thermogram with a size of 224 × 224 into 32 feature maps.

result of the input image with a specific kernel. White pixels represent strong positive activations, black pixels represent strong negative activations, and gray pixels a less strong activations on the input image. A white pixel at some locations in a channel indicates that the channel is strongly activated at that position [103].

As shown in Figure 8, some feature maps provide important information on the input image, whereas other maps fail to describe the value of the feature extracted. This indicates that some kernels fail to detect the significant information in textural features. Interpretation of feature mapping results indicates which kernel strongly extracts the input feature. Assigning a good kernel should reduce the training time necessary to learn the input feature, thus making the simulation more rapid.

2) FULLY-CONNECTED LAYER

Feature maps resulting from the convolutional layer are in the form of a multidimensional array. Thus, it is necessary to flatten or reshape the feature map into a one-dimensional array (vector) before it is used as the input for the fully connected layer. In other words, fully connected layers correspond to convolutional layers with a filter size of 1×1. A fully-connected layer is also known as a dense layer, in which each input is connected to each output by learnable weights. When features are extracted by convolutional layers and down-sampled by pooling layers, they are mapped by a subset of fully-connected layers to the final outputs of the network, such as probabilities of each class in classification tasks. The final fully-connected layer typically has the same number of output nodes as classes [104].

C. IMAGE CLASSIFICATION

Image classification is the process of classifying images according do their visual content. The training process for NNs involves recognizing breast thermograms with given label e.g., healthy and cancer. This challenge is known as supervised learning [105].

When classifying an object into different categories, CNNs often make decision from a probabilistic point of view, which is termed inference. This means that output probabilities will be an array of numbers between 0 and 1. One common type of output model is the softmax function which calculates the probability distribution of an event. In CNNs, the softmax function calculates the probability of an output image over the possible target classes. The softmax function is defined as follows [104]:

$$\sigma(z)_j = \frac{\exp(z_j)}{\sum_{k=1}^{K} \exp(z_k)} \quad \text{for } j = 1, \cdots, K, \tag{6}$$

where z_j is a number of inputs layer to the output layer and k indexes of the output units.

D. BACKPROPAGATION

Backpropagation is performed in the final layer of CNNs and is used only during training. Here, NNs learn from errors during training. This process updates weights such that the biases are zero based on the difference in the target output (ground truth) and predicted output. Loss and optimization functions are applied to reduce the bias (error). The mean square error and common loss function in the classification problem involves a cross-entropy loss defined as follows [79]:

$$L(p, y) = -\sum y_n \log(p_n), \quad n \in [1, N] \tag{7}$$

where y denotes target output, p is the probability of each output class, and n denotes the neurons. There is a total N neurons, therefore $\mathbf{p}, \mathbf{y} \in \mathbf{R^N}$. The probability of each class can be calculated using the softmax function.

An optimization algorithm is applied to reduce loss. Currently, the most popular optimizer in training samples is the stochastic gradient descent (SGD) given that it performs a parameter update for each training sample [106]. Considerable amount of research has aimed to accelerate gradient descent, such as limited-BFGS [107], parallelized SGD [108], and stochastic variance reduced gradient [109]. In 2014 Adam optimizer was introduced as superior optimizer for used in training DNNs [110]. The Adam optimizer requires low memory and is an adaptive learning rate optimizer. Nonetheless, in some cases, SGD exhibits better result. Since then, many studies have been conducted to address the limitation of the Adam optimizer such as Adagrad [111] and RMSProp [112].

V. RESEARCH ON BREAST THERMOGRAM CLASSIFICATION

In a cohort study in 2002, E. Y. K. Ng initiated works of early breast cancer detection using NNs [38]. Four backpropagation NNs were developed to examine the accuracy of detection based on breast thermograms. This examination classified the breast cases into normal, benign, and malignant groups. Although its accuracy rate was poor, this study confirmed the potential of using breast thermograms with NNs to detect breast cancer at an early stage. Subsequently, more approaches were developed, as shown in Table 4.

In 2004, Jakubowska applied artificial NN (ANN) with non-linear discriminant analysis (NDA) [113]. This technique was found to reduce false positive errors. In the same year, Koay implemented two backpropagation techniques of ANN, resilient backpropagation, and Levenberg-Marquardt (LM) algorithms [59]. Backpropagation NNs were trained using 18 images and validated with 19 breast thermograms. Input data comprise five statistical parameters from two conditions, whole breast and breast quadrant. The ANN with the LM algorithm showed the best results by correctly predicting all images with breast quadrant statistics.

In 2008, an advanced integrated technique of artificial NNs and bio-statistics was conducted in [114]. They implemented ANN of radial basis function network (RBFN). The prediction in identifying breast cancer in healthy and cancerous classes resulted 80.95% for accuracy rate with 100% sensitivity and 70.6% specificity.

Acharya *et al.* applied SVM to classify breast thermograms into normal and malignant [115]. Textural features extracted from the co-occurrence matrix were fed into the SVM classifier and resulting in an accuracy of 88.10%. The study [116] compared these three classifiers: SVM, Naïve Bayes, and k-NN. Twenty textural features based on GLCM were

TABLE 4. Works on breast thermogram classification using artificial neural networks.

Study	Classifier	Result
E. Y. K. Ng. et al., 2002 [38]	ANN	Accuracy of diagnosing breast cancer 61.54%
Jakubowska et al., 2004 [113]	ANN + NDA	Classes were not separated well
Koay et al., 2004 [59]	BP ANN + RP BP ANN + LM	Whole breast: one image misclassified both for ANN using LM and RP Breast quadrant: all images classified correctly using LM
E. Y. K. Ng and E. C. Kee, 2008 [114]	ANN + RBFN	Accuracy 80.95%
Acharya et al., 2012 [115]	SVM	Accuracy 88.10%
Milosevic et al., 2014 [116]	SVM, Naïve Bayes, and k-NN	SVM accuracy 85% Naïve Bayes accuracy 80% k-NN accuracy 92.5%
Sathish et al., 2016 [89]	SVM RBF	Accuracy 90%
Nicandro et al. 2013 [117]	Bayesian network	Accuracy 71.88%
EtehadTavakol et al. 2013 [118]	Adaptive boosting	Accuracy for detecting malignant cases 95%

used to group the negative and positive masses of breast. The resulting accuracy rates were 85%, 80%, and 92.5% for SVM, Naïve Bayes, and k-NN, respectively. A further study [89] classified normal and abnormal breast thermograms based on GLCM textural features and histograms. To improve the accuracy rate, SVM was tested with various kernel functions such as linear, radial basis function (RBF), polynomial, quadratic, and multilayer perceptron. In total, 79 data samples were used to train the algorithm, and one sample for testing. SVM RBF was found to outperforms the classification by 90% accuracy, 87.5% sensitivity, and 92.5% specificity.

In 2012, Nicandro *et al.* proposed a thermogram diagnostic technique using the Bayesian network classifier [117] allowing the visualization of interactions between chosen variables. However, their result showed a low accuracy (71.88%) and very low specificity (37%). EtehadTavakol *et al.* performed breast thermogram classification using adaptive boosting resulting in higher accuracy rate in detecting malignant and non-malignant cases 95%, and benign and normal 83%.

Throughout these studies, the objective of improving the maximum accuracy to 100% has been targeted. The optimization of NN approaches using the DL approach has motivated the implementation of the DNN model in classifying the breast thermal medical imaging. The implementation of CNN for breast cancer detection based on breast thermogram is outlined in Table 5.

In 2018, a study [119] applied the DNN model Inception-v3 [99] coupled with SVM to classify breast thermograms

TABLE 5. Works on breast thermogram classification using deep learning.

Study	Classifier	Result
Mambou et al., 2018 [119]	DNN (InceptionV3) + SVM	The confidence classification of a sick image is 0.78 and that of a healthy image is 0.94
Nasser et al., 2019 [120]	Multilayer Perceptron	Accuracy 95%
Baffa and Lattari, 2018 [121]	CNNs	Accuracy 98% for static and 95% for dynamic protocol
Roslidar et al., 2019 [122]	DenseNet201 ResNet101 MobileNetV2 ShuffleNetV2	MobileNetV2 has an accuracy of 100% for static datasets and 99.6% for dynamic datasets
Torres-Galvan et al. [123]	VGG-16 ResNet-101 AlexNet GoogLeNet VGG-19 ResNet-50 Inception-v3	VGG-16 performed best with a balanced accuracy of 91.18%
Fernández-ovies and Andrés, 2019 [124]	ResNet18 ResNet34 ResNet50 ResNet152 VGG16 VGG19	ResNet50 resulted in the highest accuracy (98.75%)
Zuluaga-Gomez et al. 2019 [94]	Proposed CNNs	Accuracy 92%
Santiago et al. 2019 [125]	Segmentation + CNN	Accuracy 100%

into binary classes: healthy and sick images. To deal with the limited breast thermogram dataset, this study applied the image pre-processing. Following pre-processing of augmentation, the breast thermograms were fed into the integrated classifier of DNN Inception-v3 [126] and SVM [127] to train the networks, but not all features were classified properly. Although this result was not completely satisfying, it represented a significant advancement in the application of DL.

A study [120] applied a multilayer perceptron DNN model to classify breast thermogram in four classes. Although its accuracy was at 95%, feature extraction was performed conventionally.

Breast infrared imaging classification was previuosly achieved by applying CNN as a classifier for static and dynamic images [121]. This research aimed to address the problem of limited datasets by conducting some pre-processing techniques. Four strategies were used to evaluate protocols of static and dynamic image acquisition [45]. The first strategy assigned all data (20 images) in a single array. The second involved use of all 20 images of a patient set and computation of their mean value. Third, the first and last images with a significant difference were chosen, and their mean was computed. The last method used image subtraction of the last and first images to produce transformed image for use as an input for the training network. These strategies enabled the reduction in the required dataset size to achieve

an effective model. In this study, the CNNs architecture comprised two convolutional layers and two max pooling layers. The output layer is a fully connected layer with two classes: healthy and unhealthy, and the networks were optimized using the Adam optimizer. The proposed model resulted in accuracies of 98% for the static protocol and 95% for the dynamic protocol.

A comparison of the performance of CNN for early detection of breast cancer based on infrared thermography was undertaken previously [124]. CNN architectures of ResNet18, ResNet34, ResNet50, ResNet152, VGG16, and VGG19 were implemented using Fast.ai and Pytorch libraries. The result of this comparison showed that ResNet34 and ResNet50 provided 100% accuracy in blind validation; however, ResNet50 was claimed to be less stable compared to ResNet34.

Another study compared CNN performance between dense and lightweight NNs [122]. The comparative study was performed by fine-tuning the pre-trained networks using the MatLab DL toolbox [90]. The pre-trained networks of ResNet101 and DenseNet201 were used as dense NNs, and MobileV2 and ShuffleNetV2 as lightweight NNs. During data training process, the results showed that MobileNetV2 outperforms all other pre-trained models in training effort, although it has lower sensitivity than deep DenseNet201.

A comparison of the performance of DL models using transfer learning was also performed [123]. Using 173 images from DMR [45], 7 CNN pre-trained architectures were compared. The CNN model VGG-16 exhibited a higher performance than AlexNet, GoogLeNet, ResNet-50, ResNet-101, Inception-v3, and VGG-19.

Recently, a study [94] demonstrated the influence of data pre-processing, data augmentation, and database size on the proposed CNN model. Augmented thermogram databases were used to train SeResNet [128], ResNet50 [129], VGG16 [98], Inception-v3 [126], InceptionResNetV2 [130], and Xception [131] CNN models. After pre-training, it was found that the simpler CNN models resulted in higher performance metrics. The authors also compared several backpropagation optimizers. The GAP layers, Adam, RMSProp, and SGD optimizer were implemented and observed during the experiment. They found that GAP layers and Adam optimizers yielded the best results. Finally, a proposed CNNs model based on the experiment result was built and was able to classify the breast thermograms with an accuracy of 92%.

Another study implemented image segmentation prior to feeding the input into CNN [125]. The thermography breast images were segmented using the combination curvature function k and gradient vector flow method. These thermograms were classified into binary classes of normal and abnormal using a CNN model based on the CNN model proposed by LeCun *et al.* [132]. Although the accuracy rate was 100%, the simulation time was not mentioned in the discussion.

Most previous studies have shown that DNNs with shallow layers perform particularly well by virtue of their ability to decrease simulation time while maintaining high accuracy. Models with shallow architectures and few parameters are robust against overfitting problems involved in DL algorithms and can harness the ability to learn data using hidden layers. Moreover, because there are only two to four classes assigned, the use of a simple CNN models is a good decision for the purpose of breast thermogram classification.

VI. FUTURE WORKS

Based on our review of the literature, it is affirmed that DL implementation in medical image classification results in higher accuracies than other neural network (NN) methods. When detecting breast cancer using DL, two crucial points must be addressed: how to detect at an early stage and use of a high accuracy rate. A DL algorithm requires large datasets to ensure 100% accuracy validation. Thus, to enable the effectiveness of DL in classifying breast thermograms, the availability of a representative dataset is essential. To enable early detection, pre-screening examination can be conducted by breast self-examination (BSE) method. Hence, a DL algorithm should be lightweight to allow the installation of an application in a portable device capable of supporting self-screening. Breast thermograms with an ROI as an input should support less computation for a lightweight model. To facilitate these requirements, we recommend that future efforts should take into account the production of the representative dataset, assembling segmentation and augmentation algorithms, assigning a good kernel, and building a lightweight CNN model.

1) REPRESENTATIVE DATASET

The availability of representative dataset is important for the training process. More datasets will increase the robustness of the training performance, taking into account the datasets used to train the CNN model. The number of training data should also be balanced for the assigned classes.

Studies addressing dataset acquisition should be conducted to support the early screening methods. Current public datasets are available in only two classes, healthy and sick, which are insufficient for comprehensive early screening. Early screening methods should ideally be capable of identifying tumors with sizes of less than 20 mm (at the pre-cancerous stage). Thus, we suggest three classes of dataset should be provided: class I comprising a healthy breast thermogram, class II comprising patients with a tumor size of less than 20 mm, class III comprising breast thermograms from patients with tumor sizes larger than 20 mm [133].

2) AUTOMATIC SEGMENTATION AND AUGMENTATION

Prior to feeding inputs into CNNs, image pre-processing of breast thermograms should be performed to facilitate a feature extraction processes. Image pre-processing at this point could include the denoizing input images and taking ROIs of

the breast thermograms. Another pre-processing that should be improved is the data augmentation.

Feeding only the ROI portion into further considerations may accelerate the feature mapping operations in the convolutional layer because only the important parts of the breast thermograms are learned. Previous studies have shown that accuracy can be increased when the input images are segmented. Thus, ROI segmentation needs to be targeted. Segmentation of breast thermogram must cover all breast tissue and nearby the ganglion area. A representative ROI could be achieved using a good segmentation algorithm. A means of automatic ROI segmentation should be built and assembled to the CNN algorithm. This would reduce computation time and may increase classification accuracy rates.

Moreover, data augmentation is an effective approach to deal with limited datasets. It allows synthetic transformations of the input. Dataset translation and similar approaches are invariant in convolution and pooling techniques. Thus, they are useful techniques for improving data learning and increasing interpretation accuracy.

3) GOOD KERNEL

CNN enables automatic feature extraction. Therefore, theoretically, determining which features characterize the healthy and cancerous image is not necessary. However, given that we consider the knowledge of important features in breast thermograms when designing a DL model, we can shorten the feature learning process. This can be achieved by assigning a good kernel that accurately maps important features. Subsequently, convolutional calculation may be minimized and classification simulation may proceed more efficiently.

4) MOBILE LIGHTWEIGHT

In supporting early stage breast cancer detection, a portable breast cancer detector has been proposed [134]. However, the NN algorithm applied here has not yet achieved 100% accuracy. Nonetheless, CNN has shown better performance in classifying images and current CNN models are built for many classes with many parameters. Because there are only between two and four classes in breast cancer detection projects, CNN can be constructed within the constraints imposed by lightweight model.

Designing a simple CNN with adequate layers and good kernels can speed up convolution computation. A lightweight mobile model will enable the development of an BSE application for a portable device. This would better enable self-screening examination for early breast cancer detection. Consequently, research should focus on integrating thermography and DL approaches in line with the development of portable screening devices.

VII. CONCLUSION

Early detection of breast cancer remains the cornerstone of breast cancer control. Breast self-examination is recommended by the World Health Organization to raise women awareness of breast cancer risks. Thermography has been proposed as an early detection screening method, and we believe that it provides a promising development towards a self-screening method that can detect breast cancer at an early stage. An overview of breast thermogram potential indicates that the early symptoms of breast cancer can be observed by identifying the asymmetrical thermal distributions between the breasts.

The asymmetrical thermal distribution on breast thermograms can be evaluated using computer-assisted technology. The use of this technology can minimize errors. Our review has shown that the current NN models have led to an increased in accuracy of breast cancer thermogram classification, particularly in distinguising between healthy and cancerous cases. Nevertheless, the performance of the NNs model must be improved.

Future research needs to work toward improved classification of breast thermograms. This will require providing representative datasets, preparing good ROIs, assigning good kernels, implementing lightweight CNN models. Achievement of these objectives will shorten the time involved in convolution computation and increase accuracy rates. A risk-free screening method using thermography could then be proposed for self-breast screening method at an early stage without requiring physical involvement.

REFERENCES

[1] IAFR Cancer. *Global Cancer Observatory*. Accessed: Jun. 30, 2019. [Online]. Available: http://gco.iarc.fr/

[2] C. Nickson and A. M. Kavanagh, "Tumour size at detection according to different measures of mammographic breast density," *J. Med. Screening*, vol. 16, no. 3, pp. 140–146, Sep. 2009.

[3] S. A. Narod, "Tumour size predicts long-term survival among women with lymph node-positive breast cancer," *Current Oncol.*, vol. 19, no. 5, pp. 249–253, Sep. 2012.

[4] OncoLink Team. (Jan. 2020). *All About Breast Cancer*. [Online]. Available: https://www.oncolink.org/cancers/breast/all-about-breast-cancer

[5] *Breast Cancer: Prevention and Control*, World Health Org., Geneva, Switzerland, 2019.

[6] Z. Jiao, X. Gao, Y. Wang, and J. Li, "A deep feature based framework for breast masses classification," *Neurocomputing*, vol. 197, pp. 221–231, Jul. 2016.

[7] H. Chougrad, H. Zouaki, and O. Alheyane, "Deep convolutional neural networks for breast cancer screening," *Comput. Methods Programs Biomed.*, vol. 157, pp. 19–30, Apr. 2018.

[8] M. A. Al-Masni, M. A. Al-Antari, J.-M. Park, G. Gi, T.-Y. Kim, P. Rivera, E. Valarezo, M.-T. Choi, S.-M. Han, and T.-S. Kim, "Simultaneous detection and classification of breast masses in digital mammograms via a deep learning YOLO-based CAD system," *Comput. Methods Programs Biomed.*, vol. 157, pp. 85–94, Apr. 2018.

[9] J. Arevalo, F. A. González, R. Ramos-Pollán, J. L. Oliveira, and M. A. G. Lopez, "Representation learning for mammography mass lesion classification with convolutional neural networks," *Comput. Methods Programs Biomed.*, vol. 127, pp. 248–257, Apr. 2016.

[10] N. Dhungel, G. Carneiro, and A. P. Bradley, "The automated learning of deep features for breast mass classification from mammograms," in *Proc. Int. Conf. Med. Image Comput. Comput.-Assist. Intervent.* Cham, Switzerland: Springer, 2016.

[11] M. G. Ertosun and D. L. Rubin, "Probabilistic visual search for masses within mammography images using deep learning," in *Proc. IEEE Int. Conf. Bioinf. Biomed. (BIBM)*, Nov. 2015, pp. 1310–1315.

[12] J. Gallego-Posada, D. A. Montoya-Zapata, and O. L. Quintero-Montoya "Detection and diagnosis of breast tumors using deep convolutional neural networks," in *Proc. 17th Latin Amer. Conf. Automat. Control*, 2011, pp. 1–9.

[13] T. Kooi, G. Litjens, B. van Ginneken, A. Gubern-Mérida, C. I. Sánchez, R. Mann, A. den Heeten, and N. Karssemeijer, "Large scale deep learning for computer aided detection of mammographic lesions," *Med. Image Anal.*, vol. 35, pp. 303–312, Jan. 2017.

[14] A. Akselrod-Ballin, L. Karlinsky, S. Alpert, S. Hasoul, R. Ben-Ari, and E. Barkan, "A region based convolutional network for tumor detection and classification in breast mammography," in *Proc. Int. Workshop Deep Learn. Med. Image Anal. Int. Workshop Large-Scale Annotation Biomed. Data Expert Label Synth.*, 2016, pp. 197–205.

[15] B. Q. Huynh, H. Li, and M. L. Giger, "Digital mammographic tumor classification using transfer learning from deep convolutional neural networks," *J. Med. Imag.*, vol. 3, no. 3, Aug. 2016, Art. no. 034501.

[16] Y. Qiu, Y. Wang, S. Yan, M. Tan, S. Cheng, H. Liu, and B. Zheng, "An initial investigation on developing a new method to predict short-term breast cancer risk based on deep learning technology," *Proc. SPIE*, vol. 9785, Mar. 2016, Art. no. 978521.

[17] A. S. Becker, M. Marcon, S. Ghafoor, M. C. Wurnig, T. Frauenfelder, and A. Boss, "Deep learning in mammography: Diagnostic accuracy of a multipurpose image analysis software in the detection of breast cancer," *Investigative Radiol.*, vol. 52, no. 7, pp. 434–440, Jul. 2017.

[18] A. Rakhlin, A. Shvets, V. Iglovikov, and A. A. Kalinin, "Deep convolutional neural networks for breast cancer histology image analysis," in *Proc. Int. Conf. Image Anal. Recognit.* Cham, Switzerland: Springer, 2018, pp. 737–744.

[19] D. Bardou, K. Zhang, and S. M. Ahmad, "Classification of breast cancer based on histology images using convolutional neural networks," *IEEE Access*, vol. 6, pp. 24680–24693, 2018.

[20] A. Cruz-Roa, A. Basavanhally, F. González, H. Gilmore, M. Feldman, S. Ganesan, N. Shih, J. Tomaszewski, and A. Madabhushi, "Automatic detection of invasive ductal carcinoma in whole slide images with convolutional neural networks," *Proc. SPIE*, vol. 9041, Mar. 2014, Art. no. 904103.

[21] Q. Zhang, Y. Xiao, W. Dai, J. Suo, C. Wang, J. Shi, and H. Zheng, "Deep learning based classification of breast tumors with shear-wave elastography," *Ultrasonics*, vol. 72, pp. 150–157, Dec. 2016.

[22] S. V. Fotin, Y. Yin, H. Haldankar, J. W. Hoffmeister, and S. Periaswamy, "Detection of soft tissue densities from digital breast tomosynthesis: Comparison of conventional and deep learning approaches," *Proc. SPIE*, vol. 9785, Mar. 2016, Art. no. 97850X.

[23] R. K. Samala, H.-P. Chan, L. Hadjiiski, M. A. Helvie, J. Wei, and K. Cha, "Mass detection in digital breast tomosynthesis: Deep convolutional neural network with transfer learning from mammography," *Med. Phys.*, vol. 43, no. 12, pp. 6654–6666, Nov. 2016.

[24] R. K. Samala, H.-P. Chan, L. Hadjiiski, K. Cha, and M. A. Helvie, "Deep-learning convolution neural network for computer-aided detection of microcalcifications in digital breast tomosynthesis," *Proc. SPIE*, vol. 9785, Mar. 2016, Art. no. 97850Y.

[25] X. Zhou, T. Kano, H. Koyasu, S. Li, T. Hara, X. Zhou, M. Matsuo, and H. Fujita, "Automated assessment of breast tissue density in non-contrast 3D CT images without image segmentation based on a deep CNN," *Proc. SPIE*, vol. 10134, Mar. 2017, Art. no. 101342Q.

[26] H. Li, J. Weng, Y. Shi, W. Gu, Y. Mao, Y. Wang, W. Liu, and J. Zhang, "An improved deep learning approach for detection of thyroid papillary cancer in ultrasound images," *Sci. Rep.*, vol. 8, no. 1, pp. 1–12, Dec. 2018.

[27] American College of Obstetricians and Gynecologists, "Breast cancer risk assessment and screening in average-risk women," *Pract. Bull.*, no. 179, 2017.

[28] *Mammography*. Accessed: Oct. 5, 2019. [Online]. Available: https://www.nibib.nih.gov/science-education/science-topics/mammography

[29] L. Glassman, "Evaluation of breast calcifications," *J. Radiol.*, vol. 90, no. 10, pp. 1306–1307, Oct. 2009.

[30] D. L. Preston, A. Mattsson, E. Holmberg, R. Shore, N. G. Hildreth, and J. D. Boice, "Radiation effects on breast cancer risk: A pooled analysis of eight cohorts," *Radiat. Res.*, vol. 158, no. 2, pp. 220–235, Aug. 2002.

[31] P. M. Arabi, S. Muttan, and R. J. Suji, "Image enhancement for detection of early breast carcinoma by external irradiation," in *Proc. 2nd Int. Conf. Comput., Commun. Netw. Technol.*, Jul. 2010, pp. 1–9.

[32] S. G. Orel, M. D. Schnall, C. M. Powell, M. G. Hochman, L. J. Solin, B. L. Fowble, M. H. Torosian, and E. F. Rosato, "Staging of suspected breast cancer: Effect of MR imaging and MR-guided biopsy," *Radiology*, vol. 196, no. 1, pp. 115–122, Jul. 1995.

[33] V. Kalles, G. C. Zografos, X. Provatopoulou, D. Koulocheri, and A. Gounaris, "The current status of positron emission mammography in breast cancer diagnosis," *Breast Cancer*, vol. 20, no. 2, pp. 123–130, 2013.

[34] Q. Huang, F. Zhang, and X. Li, "Few-shot decision tree for diagnosis of ultrasound breast tumor using BI-RADS features," *Multimedia Tools Appl.*, vol. 77, no. 22, pp. 29905–29918, Nov. 2018.

[35] T. B. Borchartt, A. Conci, R. C. F. Lima, R. Resmini, and A. Sanchez, "Breast thermography from an image processing viewpoint: A survey," *Signal Process.*, vol. 93, no. 10, pp. 2785–2803, Oct. 2013.

[36] M. Gautherie and C. M. Gros, "Breast thermography and cancer risk prediction," *Cancer*, vol. 45, no. 1, pp. 51–56, Jan. 1980.

[37] J. M. Dixon, *ABC of Breast Diseases*. Hoboken, NJ, USA: Wiley, 2012.

[38] E. Y.-K. Ng, S. C. Fok, Y. C. Peh, F. C. Ng, and L. S. J. Sim, "Computerized detection of breast cancer with artificial intelligence and thermograms," *J. Med. Eng. Technol.*, vol. 26, no. 4, pp. 152–157, Jan. 2002.

[39] R. Gade and T. B. Moeslund, "Thermal cameras and applications: A survey," *Mach. Vis. Appl.*, vol. 25, no. 1, pp. 245–262, Jan. 2014.

[40] B. F. Jones, "A reappraisal of the use of infrared thermal image analysis in medicine," *IEEE Trans. Med. Imag.*, vol. 17, no. 6, pp. 1019–1027, Dec. 1998.

[41] E. Y.-K. Ng, "A review of thermography as promising non-invasive detection modality for breast tumor," *Int. J. Thermal Sci.*, vol. 48, no. 5, pp. 849–859, May 2009.

[42] R. G. Miller, "Breast cancer screening: Can we talk?" *J. Gen. Internal Med.*, vol. 16, no. 3, pp. 206–207, Mar. 2001.

[43] H. Qi and N. A. Diakides, "Thermal infrared imaging in early breast cancer detection," in *Augmented Vision Perception in Infrared*. London, U.K.: Springer, 2009, pp. 139–152.

[44] M. Garduño-Ramón, S. Vega-Mancilla, L. Morales-Henández, and R. Osornio-Rios, "Supportive noninvasive tool for the diagnosis of breast cancer using a thermographic camera as sensor," *Sensors*, vol. 17, no. 3, p. 497, Mar. 2017.

[45] L. F. Silva, D. C. M. Saade, G. O. Sequeiros, A. C. Silva, A. C. Paiva, R. S. Bravo, and A. Conci, "A new database for breast research with infrared image," *J. Med. Imag. Health Informat.*, vol. 4, no. 1, pp. 92–100, Mar. 2014.

[46] R. R. Devi and G. S. Anandhamala, "Recent trends in medical imaging modalities and challenges for diagnosing breast cancer," *Biomed. Pharmacol. J.*, vol. 11, no. 3, pp. 1649–1658, Sep. 2018.

[47] M. Gautherie, "Atlas of breast thermography with specific guidelines for examination and interpretation," PAPUSA, Milan, Italy, Tech. Rep., 1989, vol. 256.

[48] S. T. Kakileti, G. Manjunath, H. Madhu, and H. V. Ramprakash, "Advances in breast thermography," in *New Perspectives in Breast Imaging*. London, U.K.: IntechOpen, 2017, p. 91.

[49] J. R. Keyserlingk, P. D. Ahlgren, E. Yu, and N. Belliveau, "Infrared imaging of the breast: Initial reappraisal using high-resolution digital technology in 100 successive cases of stage I and II breast cancer," *Breast J.*, vol. 4, no. 4, pp. 245–251, Jul. 1998.

[50] M. Kontos, R. Wilson, and I. Fentiman, "Digital infrared thermal imaging (DITI) of breast lesions: Sensitivity and specificity of detection of primary breast cancers," *Clin. Radiol.*, vol. 66, no. 6, pp. 536–539, Jun. 2011.

[51] R. Omranipour, A. Kazemian, S. Alipour, M. Najafi, M. Alidoosti, M. Navid, A. Alikhassi, N. Ahmadinejad, K. Bagheri, and S. Izadi, "Comparison of the accuracy of thermography and mammography in the detection of breast cancer," *Breast Care*, vol. 11, no. 4, pp. 260–264, 2016.

[52] *Thermology*. Accessed: Oct. 5, 2019. [Online]. Available: https://www.thermology.com/history.htm

[53] A. Ramírez-Torres, R. Rodríguez-Ramos, F. J. Sabina, C. García-Reimbert, R. Penta, J. Merodio, R. Guinovart-Díaz, J. Bravo-Castillero, A. Conci, and L. Preziosi, "The role of malignant tissue on the thermal distribution of cancerous breast," *J. Theor. Biol.*, vol. 426, pp. 152–161, Aug. 2017.

[54] R. N. Lawson, "A new tool in the investigation of breast cancer," *Can. Serv. Med. J.*, vol. 13, pp. 517–518, 1957.

[55] H. H. Liu and Z. Q. Liu, "Thermal texture mapping—A new way of evaluating thermal signatures of the body and holistic interpretation of infrared images," in *Medical Infrared Imaging*. Boca Raton, FL, USA: CRC Press, 2013.

[56] C. Yuan, C. Wang, and S. T. Song, "Thermal texture mapping in breast cancer," *Chin. J. Med. Imag. Technol.*, vol. 16, no. 1, pp. 7–10, 2006.

[57] Z. Shang and G. Jiang, "Fundamental theoretic research of thermal texture maps I—Simulation and analysis of the relation between the depth of inner heat source and surface temperature distribution in isotropy tissue," in *Proc. 26th Annu. Int. Conf. IEEE Eng. Med. Biol. Soc.*, Sep. 2004, pp. 5271–5273.

[58] M. K. Bhowmik, U. R. Gogoi, G. Majumdar, D. Bhattacharjee, D. Datta, and A. K. Ghosh, "Designing of ground-truth-annotated DBT-TU-JU breast thermogram database toward early abnormality prediction," *IEEE J. Biomed. Health Informat.*, vol. 22, no. 4, pp. 1238–1249, Jul. 2018.

[59] J. Koay, C. Herry, and M. Frize, "Analysis of breast thermography with an artificial neural network," in *Proc. 26th Annu. Int. Conf. IEEE Eng. Med. Biol. Soc.*, vol. 1, Sep. 2004, pp. 1159–1162.

[60] E. Y. K. Ng and E. C. Kee, "Integrative computer-aided diagnostic with breast thermogram," *J. Mech. Med. Biol.*, vol. 7, no. 1, pp. 1–10, Mar. 2007.

[61] N. Arora, D. Martins, D. Ruggerio, E. Tousimis, A. J. Swistel, M. P. Osborne, and R. M. Simmons, "Effectiveness of a noninvasive digital infrared thermal imaging system in the detection of breast cancer," *Amer. J. Surg.*, vol. 196, no. 4, pp. 523–526, Oct. 2008.

[62] X. Tang, H. Ding, Y.-E. Yuan, and Q. Wang, "Morphological measurement of localized temperature increase amplitudes in breast infrared thermograms and its clinical application," *Biomed. Signal Process. Control*, vol. 3, no. 4, pp. 312–318, Oct. 2008.

[63] G. C. Wishart, M. Campisi, M. Boswell, D. Chapman, V. Shackleton, S. Iddles, A. Hallett, and P. D. Britton, "The accuracy of digital infrared imaging for breast cancer detection in women undergoing breast biopsy," *Eur. J. Surgical Oncol.*, vol. 36, no. 6, pp. 535–540, Jun. 2010.

[64] O. D. Nurhayati, A. Susanto, T. S. Widodo, and M. Tjokronagoro, "Principal component analysis combined with first order statistical method for breast thermal images classification," *Int. J. Comput. Sci. Technol.*, vol. 2, no. 2, pp. 12–18, 2011.

[65] PROENG. (2012). *Image Processing and Image Analyses Applied to Mastology*. [Online]. Available: http://visual.ic.uff.br/en/proeng/

[66] N. Golestani, M. EtehadTavakol, and E. Y. K. Ng, "Level set method for segmentation of infrared breast thermograms," *EXCLI J.*, vol. 13, pp. 241–251, Mar. 2014.

[67] *Ann Arbor Thermography*. Accessed: Feb. 6, 2020. [Online]. Available: http://aathermography.com

[68] *Breast Thermography*. Accessed: Feb. 6, 2020. [Online]. Available: http://www.breastthermography.com/case_studies.htm

[69] *What is Breast Thermography?* Accessed: Feb. 6, 2020. [Online]. Available: http://www.thermologyonline.org/Breast/breast_thermography_what.htm

[70] *Case Study*. Accessed: Feb. 6, 2020. [Online]. Available: https://thermographyofiowa.com/case-studies/

[71] *Sunstate Thermal Imaging*. Accessed: Feb. 6, 2020. [Online]. Available: http://www.stimaging.com.au/page5.html

[72] E. Y. K. Ng, L. N. Ung, F. C. Ng, and L. S. J. Sim, "Statistical analysis of healthy and malignant breast thermography," *J. Med. Eng. Technol.*, vol. 25, no. 6, pp. 253–263, Jan. 2001.

[73] T. Jakubowska, B. Wiecek, M. Wysocki, and C. Drews-Peszynski, "Thermal signatures for breast cancer screening comparative study," in *Proc. 25th Annu. Int. Conf. IEEE Eng. Med. Biol. Soc.*, Sep. 2003, pp. 1117–1120.

[74] A. Materka and M. Strzelecki, "Texture analysis methods—A review," Technol. Univ. Lodz, Inst. Electron., Łódź, Poland, Tech. Rep. COST B11, 1998, p. 4968, vol. 10, no. 1.

[75] R. M. Haralick, "Statistical and structural approaches to texture," *Proc. IEEE*, vol. 67, no. 5, pp. 786–804, May 1979.

[76] M. B. Al Rasyid, Yunidar, F. Arnia, and K. Munadi, "Histogram statistics and GLCM features of breast thermograms for early cancer detection," in *Proc. Int. ECTI Northern Sect. Conf. Electr., Electron., Comput. Telecommun. Eng. (ECTI-NCON)*, Feb. 2018, pp. 120–124.

[77] S. S. Haykin, *Neural Networks and Learning Machines*. Upper Saddle River, NJ, USA: Prentice-Hall, 2009.

[78] D. Groupe, *Principle of Artificial Neural Networks*. Singapore: World Scientific, 2007.

[79] S. Khan, H. Rahmani, S. A. A. Shah, and M. Bennamoun, "A guide to convolutional neural networks for computer vision," *Synth. Lect. Comput. Vis.*, vol. 8, no. 1, pp. 1–207, Feb. 2018.

[80] D. Sathish, S. Kamath, K. Prasad, and R. Kadavigere, "Role of normalization of breast thermogram images and automatic classification of breast cancer," *Vis. Comput.*, vol. 35, no. 1, pp. 57–70, Oct. 2017.

[81] J. Singh and A. S. Arora, "Automated approaches for ROIs extraction in medical thermography: A review and future directions," *Multimedia Tools Appl.*, vol. 79, pp. 15273–15296, Jan. 2019.

[82] C. A. Lipari and J. F. Head, "Advanced infrared image processing for breast cancer risk assessment," in *Proc. 19th Annu. Int. Conf. IEEE Eng. Med. Biol. Soc. Magnificent Milestones Emerg. Opportunities Med. Eng.*, vol. 2, Oct./Nov. 1997, pp. 673–676.

[83] N. Scales, C. Kerry, and M. Prize, "Automated image segmentation for breast analysis using infrared images," in *Proc. 26th Annu. Int. Conf. IEEE Eng. Med. Biol. Soc.*, Sep. 2004, pp. 1737–1740.

[84] P. T. Kuruganti and T. Phani, "Detecting breast cancer from thermal infrared images by asymmetry analysis," *Med. Med. Res.*, Feb. 2003.

[85] M. EtehadTavakol, S. Sadri, and E. Y. K. Ng, "Application of K- and fuzzy C-means for color segmentation of thermal infrared breast images," *J. Med. Syst.*, vol. 34, no. 1, pp. 35–42, Feb. 2010.

[86] Z. Jin-Yu, C. Yan, and H. Xian-Xiang, "IR thermal image segmentation based on enhanced genetic algorithms and two-dimensional classes square error," in *Proc. 2nd Int. Conf. Inf. Comput. Sci.*, vol. 2, 2009, pp. 309–312.

[87] P. Kapoor and S. V. A. V. Prasad, "Image processing for early diagnosis of breast cancer using infrared images," in *Proc. 2nd Int. Conf. Comput. Automat. Eng. (ICCAE)*, Feb. 2010, pp. 564–566.

[88] S. S. Suganthi and S. Ramakrishnan, "Anisotropic diffusion filter based edge enhancement for segmentation of breast thermogram using level sets," *Biomed. Signal Process. Control*, vol. 10, pp. 128–136, Mar. 2014. [Online]. Available: http://www.sciencedirect.com/science/article/pii/S1746809414000093

[89] D. Sathish, S. Kamath, K. Prasad, R. Kadavigere, and R. J. Martis, "Asymmetry analysis of breast thermograms using automated segmentation and texture features," *Signal, Image Video Process.*, vol. 11, no. 4, pp. 745–752, May 2017.

[90] R. R. Devi and G. S. Anandhamala, "Analysis of breast thermograms using asymmetry in infra-mammary curves," *J. Med. Syst.*, vol. 43, no. 6, p. 146, Apr. 2019.

[91] S. Pramanik, D. Bhattacharjee, and M. Nasipuri, "MSPSF: A multi-scale local intensity measurement function for segmentation of breast thermogram," *IEEE Trans. Instrum. Meas.*, vol. 69, no. 6, pp. 2722–2733, Jun. 2020.

[92] S. Pramanik, S. Ghosh, D. Bhattacharjee, and M. Nasipuir, "Segmentation of breast-region in breast thermogram using arc-approximation and triangular-space search," *IEEE Trans. Instrum. Meas.*, vol. 69, no. 7, pp. 4785–4795, Jul. 2020.

[93] A. S. Koshki, M. Zekri, M. R. Ahmadzadeh, S. Sadri, and E. Mahmoudzadeh, "Extending contour level set model for multi-class image segmentation with application to breast thermography images," *Infr. Phys. Technol.*, vol. 105, Mar. 2020, Art. no. 103174.

[94] J. Zuluaga-Gomez, Z. Al Masry, K. Benaggoune, S. Meraghni, and N. Zerhouni, "A CNN-based methodology for breast cancer diagnosis using thermal images," 2019, *arXiv:1910.13757*. [Online]. Available: http://arxiv.org/abs/1910.13757

[95] S. Dodge and L. Karam, "Understanding how image quality affects deep neural networks," in *Proc. 8th Int. Conf. Qual. Multimedia Exper. (QoMEX)*, Jun. 2016, pp. 1–6.

[96] Y. Jia, E. Shelhamer, J. Donahue, S. Karayev, J. Long, R. Girshick, S. Guadarrama, and T. Darrell, "Caffe: Convolutional architecture for fast feature embedding," in *Proc. 22nd ACM Int. Conf. Multimedia*, 2014, pp. 675–678.

[97] K. Chatfield, K. Simonyan, A. Vedaldi, and A. Zisserman, "Return of the devil in the details: Delving deep into convolutional nets," in *Proc. Brit. Mach. Vis. Conf.*, 2014, pp. 1–11.

[98] K. Simonyan and A. Zisserman, "Very deep convolutional networks for large-scale image recognition," in *Proc. Int. Conf. Learn. Represent.*, 2015, pp. 1–14.

[99] C. Szegedy, W. Liu, Y. Jia, P. Sermanet, S. Reed, D. Anguelov, D. Erhan, V. Vanhoucke, and A. Rabinovich, "Going deeper with convolutions," in *Proc. IEEE Conf. Comput. Vis. Pattern Recognit. (CVPR)*, Jun. 2015, pp. 1–9.

[100] O. Russakovsky, J. Deng, H. Su, J. Krause, S. Satheesh, S. Ma, Z. Huang, A. Karpathy, A. Khosla, M. Bernstein, A. C. Berg, and L. Fei-Fei, "ImageNet large scale visual recognition challenge," *Int. J. Comput. Vis.*, vol. 115, no. 3, pp. 211–252, Dec. 2015.

[101] R. C. Gonzalez, "Deep convolutional neural networks [lecture notes]," *IEEE Signal Process. Mag.*, vol. 35, no. 6, pp. 79–87, Nov. 2018.

[102] M. Sandler, A. Howard, M. Zhu, A. Zhmoginov, and L.-C. Chen, "MobileNetV2: Inverted residuals and linear bottlenecks," in *Proc. IEEE/CVF Conf. Comput. Vis. Pattern Recognit.*, Jun. 2018, pp. 4510–4520.

[103] M. H. Beale, M. T. Hagan, and H. B. Denmuth. *Deep Learning Toolbox User's Guide*. The MathWorks, Inc., Natick, MA, USA. Accessed: Jan. 19, 2020. [Online]. Available: https://www.mathworks.com/help/pdf_doc/deeplearning/nnet_ug.pdf

[104] R. Yamashita, M. Nishio, R. K. G. Do, and K. Togashi, "Convolutional neural networks: An overview and application in radiology," *Insights Imag.*, vol. 9, no. 4, pp. 611–629, Aug. 2018.

[105] O. Simeone, "A brief introduction to machine learning for engineers," *Found. Trends Signal Process.*, vol. 12, nos. 3–4, pp. 200–431, 2018.

[106] S. Ruder, "An overview of gradient descent optimization algorithms," 2016, *arXiv:1609.04747*. [Online]. Available: http://arxiv.org/abs/1609.04747

[107] Q. V. Le, J. Ngiam, A. Coates, A. Lahiri, B. Prochnow, and A. Y. Ng, "On optimization methods for deep learning," in *Proc. 28th Int. Conf. Mach. Learn.*, 2011, pp. 265–272.

[108] M. Zinkevich, M. Weimer, L. Li, and A. J. Smola, "Parallelized stochastic gradient descent," in *Proc. Adv. Neural Inf. Process. Syst.*, 2010, pp. 2595–2603.

[109] R. Johnson and T. Zhang, "Accelerating stochastic gradient descent using predictive variance reduction," in *Proc. Adv. Neural Inf. Process. Syst.*, 2013, pp. 315–323.

[110] D. P. Kingma and J. Ba, "Adam: A method for stochastic optimization," 2014, *arXiv:1412.6980*. [Online]. Available: http://arxiv.org/abs/1412.6980

[111] J. Duchi, E. Hazan, and Y. Singer, "Adaptive subgradient methods for online learning and stochastic optimization," *J. Mach. Learn. Res.*, vol. 12, pp. 2121–2159, Feb. 2011.

[112] T. Tieleman and G. Hinton, "Lecture 6.5-rmsprop: Divide the gradient by a running average of its recent magnitude," *COURSERA, Neural Networks Mach. Learn.*, vol. 4, no. 2, pp. 26–31, 2012.

[113] T. Jakubowska, B. Wiecek, M. Wysocki, C. Drews-Peszynski, and M. Strzelecki, "Classification of breast thermal images using artificial neural networks," in *Proc. 26th Annu. Int. Conf. IEEE Eng. Med. Biol. Soc.*, Sep. 2004, pp. 1155–1158.

[114] E. Y. K. Ng and E. C. Kee, "Advanced integrated technique in breast cancer thermography," *J. Med. Eng. Technol.*, vol. 32, no. 2, pp. 103–114, Jan. 2008.

[115] U. R. Acharya, E. Y. K. Ng, J.-H. Tan, and S. V. Sree, "Thermography based breast cancer detection using texture features and support vector machine," *J. Med. Syst.*, vol. 36, no. 3, pp. 1503–1510, Jun. 2012.

[116] M. Milosevic, D. Jankovic, and A. Peulic, "Thermography based breast cancer detection using texture features and minimum variance quantization," *EXCLI J.*, vol. 13, p. 1204, Nov. 2014.

[117] C.-R. Nicandro, M.-M. Efrén, A.-A. M. Yaneli, M.-D.-C.-M. Enrique, A.-M. H. Gabriel, P.-C. Nancy, G.-H. Alejandro, H.-R. G. de Jesús, and B.-M. R. Erandi, "Evaluation of the diagnostic power of thermography in breast cancer using Bayesian network classifiers," *Comput. Math. Methods Med.*, vol. 2013, pp. 1–10, May 2013.

[118] M. EtehadTavakol, V. Chandran, E. Y. K. Ng, and R. Kafieh, "Breast cancer detection from thermal images using bispectral invariant features," *Int. J. Thermal Sci.*, vol. 69, pp. 21–36, Jul. 2013.

[119] S. Mambou, P. Maresova, O. Krejcar, A. Selamat, and K. Kuca, "Breast cancer detection using infrared thermal imaging and a deep learning model," *Sensors*, vol. 18, no. 9, p. 2799, Aug. 2018.

[120] M. Abdel-Nasser, A. Moreno, and D. Puig, "Breast cancer detection in thermal infrared images using representation learning and texture analysis methods," *Electronics*, vol. 8, no. 1, p. 100, Jan. 2019.

[121] M. de Freitas Oliveira Baffa and L. G. Lattari, "Convolutional neural networks for static and dynamic breast infrared imaging classification," in *Proc. 31st SIBGRAPI Conf. Graph., Patterns Images*, Oct. 2018, pp. 174–181.

[122] R. Roslidar, K. Saddami, F. Arnia, M. Syukri, and K. Munadi, "A study of fine-tuning CNN models based on thermal imaging for breast cancer classification," in *Proc. IEEE Int. Conf. Cybern. Comput. Intell. (CyberneticsCom)*, Aug. 2019, pp. 77–81.

[123] J. C. Torres-Galvan, E. Guevara, and F. J. Gonzalez, "Comparison of deep learning architectures for pre-screening of breast cancer thermograms," in *Proc. Photon. North (PN)*, May 2019, pp. 1–2.

[124] F. J. Fernández-Ovies, E. S. Alférez-Baquero, E. J. de Andrés-Galiana, A. Cernea, Z. Fernández-Muñiz, and J. L. Fernández-Martínez, "Detection of breast cancer using infrared thermography and deep neural networks," in *Proc. Int. Work-Conf. Bioinf. Biomed. Eng.* Cham, Switzerland: Springer, 2019, pp. 514–523.

[125] S. Tello-Mijares, F. Woo, and F. Flores, "Breast cancer identification via thermography image segmentation with a gradient vector flow and a convolutional neural network," *J. Healthcare Eng.*, vol. 2019, pp. 1–13, Nov. 2019.

[126] C. Szegedy, V. Vanhoucke, S. Ioffe, J. Shlens, and Z. Wojna, "Rethinking the inception architecture for computer vision," in *Proc. IEEE Conf. Comput. Vis. Pattern Recognit. (CVPR)*, Jun. 2016, pp. 2818–2826.

[127] M. Pontil and A. Verri, "Properties of support vector machines," *Neural Comput.*, vol. 10, no. 4, pp. 955–974, 1998.

[128] J. Hu, L. Shen, and G. Sun, "Squeeze-and-excitation networks," in *Proc. IEEE/CVF Conf. Comput. Vis. Pattern Recognit.*, Jun. 2018, pp. 7132–7141.

[129] X. Yu, Z. Yu, and S. Ramalingam, "Learning strict identity mappings in deep residual networks," in *Proc. IEEE/CVF Conf. Comput. Vis. Pattern Recognit.*, Jun. 2018, pp. 4432–4440.

[130] C. Szegedy, S. Ioffe, V. Vanhoucke, and A. A. Alemi, "Inception-v4, inception-resnet and the impact of residual connections on learning," in *Proc. 31st AAAI Conf. Artif. Intell.*, 2017, pp. 1–7.

[131] F. Chollet, "Xception: Deep learning with depthwise separable convolutions," in *Proc. IEEE Conf. Comput. Vis. Pattern Recognit. (CVPR)*, Jul. 2017, pp. 1251–1258.

[132] Y. Lecun, L. Bottou, Y. Bengio, and P. Haffner, "Gradient-based learning applied to document recognition," *Proc. IEEE*, vol. 86, no. 11, pp. 2278–2324, Nov. 1998.

[133] *Breast Cancer: Stages*. Accessed: Jun. 30, 2019. [Online]. Available: https://www.cancer.net/cancer-types/breast-cancer/stages

[134] J. Ma, P. Shang, C. Lu, S. Meraghni, K. Benaggoune, J. Zuluaga, N. Zerhouni, C. Devalland, and Z. Al Masry, "A portable breast cancer detection system based on smartphone with infrared camera," *Vibroeng. PROCEDIA*, vol. 26, pp. 57–63, Sep. 2019.

ROSLIDAR ROSLIDAR (Member, IEEE) was born in Banda Aceh, in 1978. She received the bachelor's degree in electrical engineering from Universitas Syiah Kuala, in 2001, and the master's programme in telecommunication engineering from the University of Arkansas, USA, in 2009. She is currently pursuing the Ph.D. degree with the Doctoral School of Engineering Science, Universitas Syiah Kuala. Since 2001, she has been with the Department of Electrical and Computer Engineering, Universitas Syiah Kuala. Her research interest includes developing the e-health monitoring system-based on non-invasive technique. She is active as the Copy Editor of the National Accredited Journal of Jurnal Rekayasa Elektrika. She received the Fulbright Award for her master's degree programme, in 2006, and the scholarship from Kementrian Ristek Dikti for one semester Ph.D. Programme in Universitas Syiah Kuala, in 2019.

AULIA RAHMAN (Member, IEEE) received the bachelor's degree from the Institut Teknologi Bandung, Indonesia, in 2005, and the master's degree in automation and robotics from Technische Universitaet Dortmund (TU Dortmund), Germany, in 2011. Since 2012, he has been with the Department of Electrical Engineering, Universitas Syiah Kuala. He affiliated with the Control System Laboratory and the Embedded System Laboratory. His research interests include mobile robotics, SLAM, control systems, computer vision, and machine learning.

RUSDHA MUHARAR (Member, IEEE) received the Sarjana Teknik (Bachelor of Engineering) degree in electrical engineering from Gadjah Mada University, Indonesia, in 1999, the M.Sc. degree in electrical engineering from the Delft University of Technology (TU Delft), The Netherlands, in 2004, and the Ph.D. degree in electrical engineering from the University of Melbourne, Australia, in 2012. From November 2012 to November 2013, he was a Postdoctoral Research Fellow with the Department of Electrical and Computer Systems Engineering, Monash University, Australia. He joined the Department of Electrical Engineering, Syiah Kuala University, Indonesia, in April 2006, where he is currently a Senior Lecturer. His research interests include communications theory, signal processing for wireless communications, and machine learning.

MUHAMMAD RIZKY SYAHPUTRA (Member, IEEE) was born in Banda Aceh, in 1998. He is currently pursuing the bachelor's degree in electrical and computer engineering with Universitas Syiah Kuala, Indonesia. Since 2017, he has been a Laboratory Assistant with the Computer Network Laboratory. He joined the Manufacturing and Design Laboratory, Lamuri Robotic Team, Universitas Syiah Kuala, in 2018, where he works for the firefighting hexapod robot. His current research interests include image processing, robotic, the Internet of Things, and computer networking. He certified as Mikrotik Certified Network Associate and Mikrotik Certified Router Engineer, in 2017. He was selected as ASEAN SAP Data Science Explorer National Finalist, in 2017.

FITRI ARNIA (Member, IEEE) received the B.Eng. degree from the Universitas Sumatera Utara (USU), Medan, in 1997, the master's degree from the University of New South Wales (UNSW), Sydney, Australia, in 2004, and the Ph.D. degree from Tokyo Metropolitan University (TMU), Tokyo, Japan, in 2008. She has been with the Department of Electrical and Computer Engineering, Faculty of Engineering, Universitas Syiah Kuala (Unsyiah), since 1999, where she is currently a Professor. She was a Visiting Scholar with TMU, in 2013, and with Suleyman Demirel University (SDU), Isparta, Turkey, in 2017. Her research interests include signal, image, and multimedia information processing. She is a member of the ACM and APSIPA.

MAIMUN SYUKRI received the medical degree from the University of Airlangga, Surabaya, Indonesia, in 1988, and the Ph.D. degree in medicine from Gadjah Mada University, Yogyakarta, Indonesia, in 2014. He was trained as an Intern with the University of Airlangga. He was also trained in nephrology with Gadjah Mada University. From 2009 to 2016, he was the Head of the Internal Medicine Department, University of Syiah Kuala. He is currently a Lecturer with the Medical Faculty, University of Syiah Kuala, Banda Aceh, Indonesia. He is also a member of the Indonesian Medical Association, the Indonesian Society of Nephrology, the Indonesian Society of Internal Medicine, the Indonesian Society of Hypertension, the Asian Pacific Society of Nephrology, and the International Society of Nephrology.

BISWAJEET PRADHAN (Senior Member, IEEE) received the Habilitation degree in remote sensing from the Dresden University of Technology, Germany, in 2011. Since 2015, he has been as the Ambassador Scientist for the Alexander Humboldt Foundation, Germany. He is currently the Director of the Centre for Advanced Modelling and Geospatial Information Systems (CAMGIS), Faculty of Engineering and IT. He is also a Distinguished Professor with the University of Technology Sydney. He is an internationally established Scientist in the fields of geospatial information systems (GIS), remote sensing, image processing, complex modeling/geo-computing, machine learning and soft-computing applications, natural hazards, and environmental modeling. Out of his more than 550 articles, more than 475 have been published in science citation index (SCI/SCIE) technical journals. He has authored eight books and 13 book chapters. He was a recipient of the Alexander von Humboldt Fellowship from Germany and the Alexander von Humboldt Research Fellowship from Germany. He received 55 awards in recognition of his excellence in teaching, service, and research, since 2006, and the World Class Professor by the Ministry of Research, Technology and Higher Education, Indonesia, in 2018 and 2019. He is also an associate editor and an editorial member of more than eight ISI journals. From 2016 to 2019, he was listed as the World's Most Highly Cited Researcher by Clarivate Analytics Report as one of the world's most influential minds.

KHAIRUL MUNADI (Member, IEEE) received the B.Eng. degree in electrical engineering from the Sepuluh Nopember Institute of Technology, Surabaya, Indonesia, in 1996, and the M.Eng. and Ph.D. degrees in electrical engineering from Tokyo Metropolitan University (TMU), Japan, in 2004 and 2007, respectively. From 1996 to 1999, he was a System Engineer with Alcatel Indonesia. Since 1999, he has been a Lecturer with the Electrical and Computer Engineering Department, Universitas Syiah Kuala (Unsyiah), Banda Aceh, Indonesia, where he has been a Professor, since August 2019. From March 2007 to March 2008, he was a Visiting Researcher in information and communication systems engineering with the Faculty of System Design, TMU. He was also a Visiting Scholar with the Department of Computer Engineering, Suleyman Demirel University (SDU), Isparta, Turkey, in 2016. His research interests include multimedia signal processing, knowledge-based management, and disaster management. He is a member of APSIPA.